applied sciences

MDPI

Article

Raman Spectroscopy and Imaging Techniques Applied to Neolithic Artefacts as a Valuable Contribution to the Archaeological Research on Piacentine Sites

Laura Fracasetti [1,2,*], Sara Pescio [3], Maria Maffi [4], Paola Mazzieri [5], Patrizia Fumagalli [1], Michele Zucali [1] and Luca Trombino [1]

[1] Earth Science Department "A. Desio", University of Milan, 20133 Milano, Italy; patrizia.fumagalli@unimi.it (P.F.); michele.zucali@unimi.it (M.Z.); luca.trombino@unimi.it (L.T.)
[2] Geosciences Department, University of Padova, Via G. Gradenigo, 35131 Padova, Italy
[3] Department of Chemistry, Life Sciences and Environmental Sustainability, University of Parma, Parco Area delle Scienze 157/A, 43124 Parma, Italy; sara.pescio@unipr.it
[4] Archaeological Museum of Travo, Via del Mulino 22, 29020 Travo, Italy; maria.maffi.archeo@gmail.com
[5] Superintendence of Archaeology, Fine Arts and Landscape for the Provinces of Parma and Piacenza, Piazza San Giovanni Paolo II 5A, 43121 Parma, Italy; paola.mazzieri@cultura.gov.it
* Correspondence: laura.fracasetti@phd.unipd.it

Abstract: Archaeologists and conservation scientists join interdisciplinary projects aiming at the in-depth analysis of artefacts and the resolution of new archaeological issues, overcoming the common limits of mesoscopic observation. The aim of this research is to perform multidisciplinary research, adapting imaging techniques (RTI imaging and 3D photogrammetry) and Raman spectroscopy from their conventional field of application to study and valorise neolithic archaeological findings from Piacentine sites (Emilia-Romagna, Italy). RTI images enable the detection of a comprehensive framework of anthropic and natural traces on the object surfaces to support the hypothesis of the intended usage of artefacts. Combining qualitative and quantitative Raman spectra analysis, the specific lithological characterisation of each fragment is conducted, thereby the understanding of their probable geographic provenance is enhanced. This contributes to the identification of the External Ligurian Units as a possible primary supply area, along with the already known outcrops in the Mont Viso Massif and Voltri Group. Their potential as a powerful instrument for conservation and valorisation has been revealed by 3D models. In fact, they may enrich museum exhibits, enhancing visitors' experience through interactive engagement and guarantee the examination of artefacts by experts across the globe through online sharing, without the need for transportation and excessive manipulation.

Keywords: Raman spectroscopy; 3D photogrammetry; reflectance transformation imaging; archaeological findings; cultural heritage; Italian Neolithic

Academic Editor: Asterios Bakolas

Received: 17 December 2024
Revised: 25 January 2025
Accepted: 27 January 2025
Published: 31 January 2025

Citation: Fracasetti, L.; Pescio, S.; Maffi, M.; Mazzieri, P.; Fumagalli, P.; Zucali, M.; Trombino, L. Raman Spectroscopy and Imaging Techniques Applied to Neolithic Artefacts as a Valuable Contribution to the Archaeological Research on Piacentine Sites. *Appl. Sci.* **2025**, *15*, 1478. https://doi.org/10.3390/app15031478

1. Introduction

In recent decades, archaeological research has increasingly become a multidisciplinary project, involving archaeologists in collaboration with scientists and professionals from different disciplines including geology, geopedology, geomorphology, and technical expertise [1,2]. This collaboration tries to overcome the eventual lack of knowledge and wants to obtain significant results to improve the archaeological research [3]. The conservation scientist, as a new profession, reflects the increasing interest and represents the professional with the highest expertise in the research and valorisation activities on cultural heritage,

including archaeological artefacts [4,5]. This approach aims to integrate the object mesoscopic observation of superficial traces and raw material employed, which is a typical competency of archaeologists, with the advanced technologies derived from scientific field improvements. However, to improve the understanding of ancient artefacts and their intended usage, the so-called "Low-Power Approach" (LPA) for the first investigation of their characteristics is always required, too [6,7]. Nevertheless, artefact examination may suffer from the degree of subjectivity inherent in the description of superficial traces and from the incapability to notice all the traces by the naked eye that may be overcome through new types of observational approaches, like innovative imaging techniques (e.g., Reflectance Transformation Imaging, Photogrammetry, or Optical Microscopy) [8]. Thus, archaeology is opened up to the defined "Scientific turn" [9], which can lead to new answers to archaeological problems that usually face archaeologists and researchers.

In addition, it has been reported in recent years that there has been a notable increase in interest in the utilisation of digital tools and computer-based data analysis in the Cultural Heritage context [10] (pp. 35–46) [11]. Interestingly, new imaging techniques and 3D reconstruction technologies enable not only a new way of investigating Cultural Heritage but also new useful opportunities for their conservation and valorisation in museums [4,12]. This tendency follows the development of the so-called "3rd Cultural (digital) Revolution" [13], which includes in the real world the virtual environments generated by 3D modelling, augmented reality and the usage of smart tools (e.g., computers, tablets, touchscreens or QRcodes) connected with the WorldWideWeb.

Owing to the up-to-date technologies and the fragile conditions of the archaeological findings, the present study aims to evidence how the application of non-invasive and non-destructive analytical techniques and imaging methods, adapted from their conventional field of study, can support archaeological research. Specific techniques were employed to analyse the samples, contingent upon the peculiar inquiry submitted by archaeologists. The digital techniques' potentiality as a means of valorising archaeological findings is further examined by the introduction of digital models into the museum collections. The samples used in the case study come from an extended area, comprising the Trebbia Valley and the Tidone Valley (Piacenza, Italy), and all date back to the Neolithic age. The biggest ones (S1 and S2) do not have a specific intended usage so far. With this intention, the application of the Reflectance Transformation Imaging (RTI) methodology and the resulting RTI image serves as a tool for the first examination of anthropic and natural traces on the artefacts' surfaces with the final aim of formulating their hypothetical intended usage. In fact, the Reflectance Transformation Imaging (RTI) method is commonly employed to enhance the traces on the surfaces of different types of objects [14–19], which are already known for their specific usage in ancient times [20,21].

The other samples have a precise archaeological identification: sample R5 has been recognised as a fragment of mace and the remaining samples (R1, R2, R3, and R4) as ring bracelet sherds.

The first appearance of ring bracelets made of polished stone dates back to the early Neolithic (5.500–4.900 BC), and it is mainly widespread in northern Italy and along the high Tyrrhenian coast [22]. In Italy, manufactures that require a significant degree of technical expertise, are typical of the neolithic groups of the Po plain (Fiorano and Vhò Groups); however, they have been sporadically found in other different contexts that are related to a subsequent chronology. Ring bracelets caught the archaeologists' attention, and they have deeply studied their social significance [23,24], their morphology [23,25], and the specific raw materials exploited. Researchers agreed on the fact that rocks belonging to the so-called HP-metaophiolites category and especially the Greenstone group have been widely manufactured for their distinctive green colour [26]. The geological provenance of

these lithologies (e.g., serpentinites, praisinites, amphibolites, jadeites) is mainly localised in the Mont Viso Massif and in the Ligurian Voltri Group, where metamorphic bodies were discovered along with specific signs of extraction activities [26–32]. In addition, secondary deposits bearing HP-metaophiolite cobbles from the Voltri Group are located in the north-western Apennines area [26]. The widespread manufacturing of ring bracelets requires the establishment of commercial routes from the Alps for the Greenstone sourcing areas along with the first maritime route for the exchange of obsidian from Lipari [22,33,34]. Thus, petrographic determination of the artefacts may integrate the current knowledge about commercial trades and quarry areas. In this way, Raman spectroscopy, which is commonly employed for the study of the molecules from different materials like pottery, patinas, corrosion surfaces, pigments and inks [35], is a non-invasive and non-destructive way to identify the mineralogical composition of the artefacts and then define their petrographic determination. It is reported that Raman spectroscopy usage for archaeometry purposes has been increasing since 2000 [36] and the development of portable devices has empowered the application of physical analytical methodology for in situ analysis [37]. In the present study, a combined qualitative and quantitative approach was implemented in the mineralogical study of lithology. It is an innovation of the literature [38,39] that exclusively prefers a qualitative approach without considering the implementation of this approach along with the most precise quantitative analysis of the vibrational spectra. In particular, the quantitative approach should provide clues into the discrimination between mineralogical phases that have similar spectra curves and peak positions. Otherwise, the uniquely qualitative approach suffers from a 16% error in the matching of Raman spectra [40]. Through QGIS technologies, the geographical localisation of the primary and secondary possible sourcing areas for those specific types of rocks is conducted, avoiding field surveys.

The three-dimensional digitalisation of Cultural Heritage is mainly used for didactic purposes [41] or aerial models [42], but it may be an effective tool for the in-depth analysis of archaeological artefacts [43]. Even if this technology requires specific software at a moderate cost, photogrammetry is a valuable instrument for the application of Virtual Archaeology [13]. It allows the artefacts to be studied by different experts across the world thanks to the 3D model sharing functionality through links from online platforms, like *Sketchfab*, one of the most important at the international level [11].

General Setting of the Study Area

The present study encompasses an extended geographical area in the province of Piacenza (north-west of the Emilia-Romagna region, Italy), where the analysed lithic artefacts have been discovered (Figure 1). The Piacenza province is the conduit between the Po plain and the northern sector of the Apennines extending to the coast of Liguria (Ligurian Sea), with its four principal valleys—the Tidone Valley, the Trebbia Valley, the Nure Valley, and the Arda Valley—gradually converging to form a natural corridor. This is the reason why humans have inhabited this area since prehistory.

The geological setting of the area is undoubtedly shaped by the Apennines orogenic phenomenon, which started approximately 30 million years ago with the onset of continental subduction and continues to exert a significant influence [44,45]. The Apennines and Pre-Apennines bedrock mainly belongs to the Ligurian Domain and is predominantly composed of turbiditic sandstones with intercalated sequences of marlstones rich in calcium carbonate. The ophiolitic complex with mantle peridotites, in the form of fragments within the predominantly arenaceous-clayey sedimentary melanges or as a true basement, also characterised the area of the Internal Ligurian Units along with peridotites intruded by layered gabbros and diorite [46]. This geological setting is especially evidenced by the presence of the Perduca Stone and Parcellara Stone in Travo, on the left bank of the Trebbia

Valley. In fact, these outcrops represent a portion of the ophiolitic complex, consisting of serpentinites [47]. The piacentine Po Plain bedrock instead consists of Tertiary and Quaternary stratified alluvial deposits of gravel and silt from the infilling process of the foreland basin [48,49]. Finally, riverbanks are characterised by the stratification of often uncemented alluvial cone sediments and Quaternary alluvial deposits of gravels and sand, which are intercalated by silty sediments.

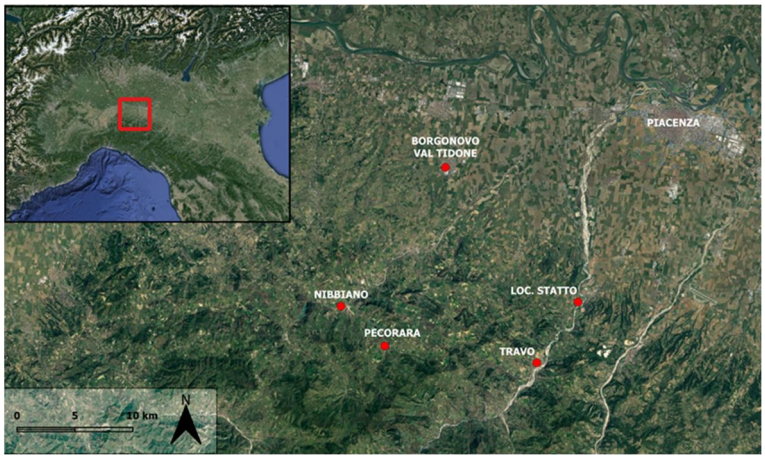

Figure 1. Google Earth image of the study area. Red dots represent the sites where archaeological findings were discovered, while the red box in the corner image localises the area within the Northern Italy.

2. Materials and Methods

2.1. Archaeological Findings

In the present study, seven lithic archaeological findings are selected from the Civic Museum of Travo and the Val Tidone Archaeological Museum in Pianello Val Tidone (Figure 2; Table 1). Their preliminary description is performed using a 30×/60× lens and a Stemi SV6 (Zeiss®) stereomicroscope equipped with optic fibres and an integrated Nikon Digital Sight DS-L1 camera for the shooting sessions.

Figure 2. (**a**) S1 and (**b**) S2 from Travo S. Andrea archaeological site (structure US1040) (**c**) Sample R1 from the Casa Gazza archaeological site (**d**) Sample R5 from fieldwalking in the locality Pecorara of Alta Val Tidone; (**e**) Sample R2 from Travo S. Andrea archaeological site; (**f**) Sample R3 from an emergency archaeological excavation in Nibbiano of Alta Val Tidone; (**g**) Sample R4 from fieldwalking in Borgonovo Val Tidone.

Table 1. Summary of the archaeological findings with their related dating, the geographical location of the discovery site and the techniques that have been employed for their examination.

Sample	Locality–Site (Valley)	Chronology	Applied Technique
S1	S. Andrea–Travo (Trebbia Valley)	"Neolitico Recente" [50]	Highlight-Reflectance Transformation Imaging
S2	S. Andrea–Travo (Trebbia Valley)	"Neolitico recente"	Highlight-Reflectance Transformation Imaging
R2	S. Andrea–Travo (Trebbia Valley)	Middle Neolithic–First VBQ	3D Photogrammetry; Raman Spectroscopy
R1	Statto–Travo (Trebbia Valley)	Early Neolithic	3D Photogrammetry; Raman Spectroscopy
R3	Nibbiano–Alta Val Tidone (Tidone Valley)	Middle Neolithic–First VBQ	3D Photogrammetry; Raman Spectroscopy
R5	Monte Fermico, Pecorara–Alta Val Tidone (Tidone Valley)	Late Neolithic	3D Photogrammetry; Raman Spectroscopy
R4	Castelnuovo and Bilegno–Borgonovo Val Tidone (Tidone Valley)	Neolithic	3D Photogrammetry; Raman Spectroscopy

Samples S1 and S2 were discovered in the S. Andrea Neolithic village in Travo, in association with three other rocks as a closure of the US 1040 structure, a subcircular hole 80 cm × 80 cm wide and 40 cm deep. They are clastic sedimentary rock with dissimilar average granulometry: S1 is predominantly sandy (0.25–1 mm, Udden–Wentworth scale) while S2 has a sandy-fine silty granulometry (0.062–0.25 mm, Udden–Wentworth scale).

The other samples were smaller and represented fragments of different lithology, conserving evidence of human manufacturing. Indeed, archaeologists agreed on the identification of R2, R3, and R4 as ring bracelet sherds, R1 as a fragment of a ring bracelet draft while R5 is considered to be a mace fragment. In detail, R2 and R3 were attributable to the A2 typology of ring bracelets while R4 was classified into the "A3 category" [23]. R1 had a rough surface and a much more irregular shape than the other artefacts which had polished surfaces. It was unearthed in 1984 in the Casa Gazza sites, located in Travo in the Statto locality; the site was characterised by a bilobate archaeological structure measuring about 1 m in depth and 10 m × 6 m which was widely studied and finally identified as a Neolithic dwelling employed between the VI and the V millennia B.C. [51]. By the observation of the fracture surfaces, all the archaeological findings showed a foliated or moderate foliated structure (R1, R2, R4), except for R3, which was characterised by a weak foliated structure.

2.2. Highlight-Reflectance Transformation Imaging (H-RTI)

The production of RTI models was achieved in two main steps: firstly, the acquisition of shots in Highlight modality and secondly their elaboration using RelightLab software (Relight (cnr.it); v2023.02). Before the acquisition of the shots, the surface of every artefact was gently washed under water flux through the slight pressure of a brush to remove undesirable deposits. To ensure complete drying, the artefacts were exposed to a heating treatment at 70 °C for 8 h in an open oven. Before every shooting session, to remove residuals, the surfaces were polished again using a dry brush.

The Highlight-RTI methodology required the construction of a virtual dome through the manual movements of a flash lamp around the object subjected to the shooting session, which was fixed in its position on the ground. The fixed scheme for the manual flash lamp positioning was designed to achieve the highest homogeneity of surface illumination and reduce the errors of the final models [52]; for this reason, the height from the floor and the

angle drawn with the object surface of the flash lamp were mathematically calculated as Fiorini (2018) [53] suggests. The constancy over time of the distances mentioned above was ensured by employing a laser telemeter. The specific guide released by the organisation [54] provides a detailed explanation of the image capture methodology.

The photographic session was conducted using a Canon EOS RP camera with an RF 24–105 mm IS STM lens and a CMSO full-frame 26.2 megapixel sensor, fixed perpendicularly to the object surface by a Manfrotto 055XPROb tripod. The synchronisation of the camera with the bulb flash-lamp Quadralite Reporter 360 TTLc (colour temperature: 5600 ± 200 °K) was performed by a Quadralite Navigator Xc trigger. Every shot framing had a uniform black background and included a metric target as well as two black reflective spheres of 1.4 cm in diameter which enabled the processing software to calculate the light direction of every photographic image [16]. Only one shot for every session, captured with the perpendicular illumination from the flash lamp, was performed by the X-RITE ColorChecker introduction into the frame. This shot allowed us to execute the eventual colour correction of the entire shooting files. For every analysed surface, 96 remote shots were performed adopting the Canon Camera Connect application. The camera shooting parameters, summarised in Table 2, were defined to ensure the highest image quality and had to be maintained at a constant value during the entirety of the photographic session. Every shot was saved in two formats: the .jpg and the raw file format, .cr3.

Table 2. The camera and flash lamp parameters used for each artefact shooting session are reported.

	Parameters	S1	S2
CAMERA	ISO	100	100
	Focal length	50	70
	Aperture (f/stop)	1/16	1/16
	Exposure time	1/160 s	1/160 s
FLASH LAMP	Power	1/16	1/16
	Flash time	1/4255 s	1/4255 s

The image processing was performed in RelightLab adopting the available algorithms with the highest coefficient number to guarantee the best quality of the final model [55]: Polynomial Texture Maps (PTM18) and Hemispheric Harmonics Maps (HSH27).

RTIViewer software (v1.1.0) [56] was employed for the visualisation of the resulting models. It allowed users to interactively change the apparent direction of surface lighting to emphasise superficial traces that were not visible to the naked eye. The mathematical transformations and enhancement modes (e.g., Normal Visualization, Specular Enhancement, Diffuse Gain, Normal Upsharp Masking) offered by the software were used to emphasise surface features.

The surface analysis and superficial traces description were conducted using the method developed by Toma (2018–2019) [57] for the same object typology. The surface was divided into four quarters and all the noticeable features were marked with specific signs. The classification of evidence was based on the determination of two main criteria: the trace origin, which may be natural or anthropic, and the chronology of formation, which was subdivided into ancient, recent, or modern traces. Calcium carbonate concretions as a reference element enabled the differentiation of ancient traces from recent and modern ones.

2.3. 3D Photogrammetry

Three-dimensional models were created through the Structure-for-Motion technology based on the capture of photos of an object and the subsequent processing of the images

using the Agisoft Metashape software (v1.8.0). The initial step of image acquisition was crucial, as the accuracy of the 3D model is contingent on the photo quality. The shooting session was performed using a Canon EOS RP camera fixed on a Manfrotto 055PRO3 tripod. The camera was equipped with an RF 24–105 mm IS STM lens, a CMSO full-frame 26.2 megapixel sensor, and a camera remote for the shutter control.

Samples were set on a rotating platform through a piece of kneaded eraser, which did not cause surface alteration and is widely employed in archaeological research [58,59] because it preserves the artefacts from damage while guaranteeing stability during experiments. As visible in Figure 3a, markers directly provided by Agisoft Metashape software (Tools < markers < print markers) must be fixed close to the sample as reference points for the subsequent image processing; with the same intention, a short sequence of letters was stuck onto the lateral surfaces of the kneaded eraser. The correct homogeneous illumination of the sample surface was ensured by a white background and two fluorescent studio lamps (Fotobestway ES-755), set at approximately 45° relative to the plane on which the object was placed. A ColorChecker X-RITE was employed for the eventual colour correction of an entire shooting file. The camera shooting parameters and the camera–object distance were calculated using the online software DoFmaster (https://www.dofmaster.com/dofjs.html (accessed on 11 March 2024), inserting the measurable depth of the object and the chosen camera focal length. Table 3 reports the overall number of photos captured for each sample along with the specific camera setting parameters, which must be maintained at a constant value during the entirety of the photographic session.

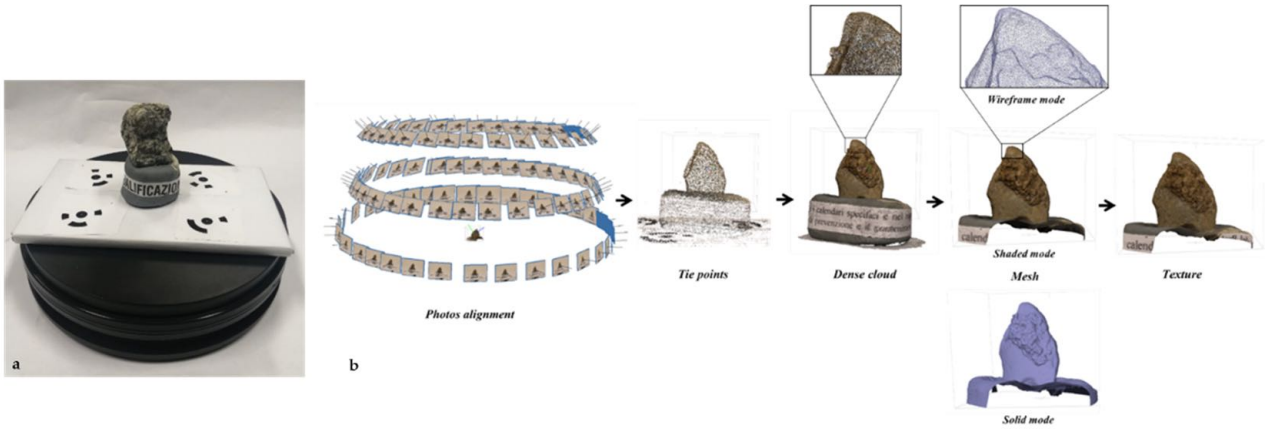

Figure 3. (**a**) The sample R5 correctly positioned within the designed set for the shooting session; (**b**) Schematic representation reporting the steps involved in the Agisoft metashape workflow to create one chunk of the R2 three-dimensional model.

Table 3. The camera parameters used for the shooting sessions related to each sample are reported.

	R5	R3	R2	R4	R1
ISO	400	400	400	250	400
focal length	105 mm	105 mm	105 mm	105 mm	105 mm
f/stop	f/22	f/22	f/25	f/22	f/25
Shutter speed	1/25 s	1/25 s	1/30 s	1/25 s	1/25 s
Camera-object distance	96.4 cm	94.6 cm	60 cm	80 cm	90 cm
Overall photos	257	248	193	273	279

Every sample required two different photo shooting sessions, in which all the aforementioned reference points (markers and sequence of letters) needed to be changed; the first session differed from the second one by 180° rotation of the sample around its horizontal axis. Each session comprised three series of photographs, captured at 0°, 45°, and 60° relative to the horizontal plane on which the sample was placed. Each series comprised photos captured at 10° progressive intervals with the sample undergoing a rotation around its vertical axis. All the photos were stored in two formats: the commonly used .jpg and the raw file format, .cr3.

The Agisoft Metashape workflow (see Figure 3b) for the three-dimensional model creation from a set of 2D images comprised: 1. Preprocessing of the imagery dataset by the quantitative evaluation of the image quality; 2. Camera alignment; 3. Sparse point reconstruction of the surface (Tie Points); 4. Dense point cloud generation; 5. Mesh generation; 6. Texture generation. A comprehensive report of the technical parameters employed for model realisation is presented in File S1.

The correction of potential mesh deficiencies or lack of texture was conducted using MeshLab and Meshmixer. The final models were downloaded on the international sharing platform of 3D models, Sketchfab, along with a brief descriptive caption for each sample.

2.4. Raman Spectroscopy

Raman spectra were collected using a bench spectrometer available at the Earth Sciences Department of the University of Milano (MI). The instrument was a LabRAM HR Evolution (Horiba®, Turin, Italy equipped with a cooled CCD detector sensor and an Nd-Yag 532 nm/100 mW laser, which generated a spot of 2 μm diameter on the sample surface. The excitation source and collection optics were arranged in a coaxial configuration and the scattered light was collected by a 50x objective (NA = 0.5; resolution = 0.65 μm) in backscattering geometry (Figure 4). The Schott KL 1600 LED lamp (colour temperature = 5600 °K) allowed sample illumination during the preliminary surface observation. The main peak of a pure silicon chip at 520.63 cm^{-1} was used to calibrate the system before data acquisition. Sample positioning under the objective was enabled by a motorised sample plate, which was guided using a 4-axis remote joystick (Marzhauser Wetzlar®, Wetzlar, Germany) connected to the computer via TANGO 4 Desktop controller (Marzhauser Wetzlar®, Wetzlar, Germany). For each point of interest on the surfaces of the samples, a spectrum was collected in the fingerprint range of 100 to 1200 cm^{-1} and in the range of 3200–3600 cm^{-1} to detect the hydroxyl group vibrational modes of water molecules within the investigated minerals [60]. A minimum of 30 spectra were collected for each archaeological artefact, except for the MFP sample, due to the irregularity of its surface (see Figure A1 in Appendix A). Three accumulations and a variable exposure time from 5 to 15 s, depending on the entity of the background fluorescence and the Raman scattering efficiency, were adopted to obtain a significant signal-to-noise ratio. Spectra were first visualised and stored using LabSpec6 Spectroscopy Suite software (v1) while the subsequent spectral processing was carried out using OriginLab. The processing was performed with manual polynomial baseline subtraction and the Lorentzian fitting of the spectral curves.

The first qualitative study was conducted for both the leucocratic and the melanocratic fractions by direct comparison of the acquired spectra with the international Raman database RRUFF using CrystalSleuth software (v1.0). The discrimination between amphibole and pyroxene was also performed by observing the positions of the Raman peaks in the 3.200–3.600 cm^{-1} interval, which are related to the presence of the hydroxyl group (-OH).

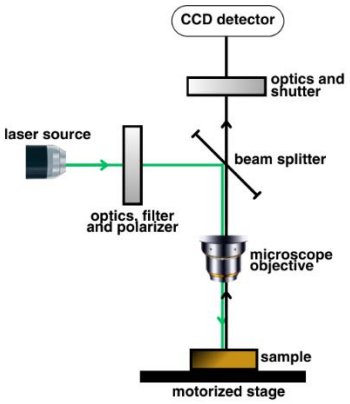

Figure 4. Schematics of the Raman spectroscopy system. The laser beam is shown in green while the Raman scattered signal is shown in black.

For the spectra identified as belonging to the plagioclase fraction, a quantitative analysis was performed using the method described by Bersani et al. (2018) [61]. In the present study, the selected peaks for anorthite content ($An_{(mol\%)}$) evaluation were ν_b at about 478 cm^{-1} and ν_a at 507 cm^{-1}. To preliminarily individuate the position of the investigated mineral in the plagioclase solid solution, the centroid distance (Δ_{ab}) between ν_a and ν_b was calculated. Then, the An(mol%) was obtained using Equation (1) if the mineral has a Δ_{ab} less than 27 cm^{-1}, while Equation (2) was used if Δ_{ab} exceeds 27 cm^{-1}, considering the ν_a peak width Γ_a as a reference parameter. Equations (1) and (2) result from the linear regression of data derived from plagioclase minerals with known An(mol%) content. They clearly express the relationship between the An(mol%) content and the measurable Δ_{ab} and Γ_a for the selected ν_a and ν_b peaks, and thus the equations enable the characterisation of unknown plagioclase by their An(mol%) content.

$$An_{(mol\%)} = -3.20 \cdot \Delta_{ab} + 147.8, \quad (1)$$

$$An_{(mol\%)} = 4.26 \cdot \Gamma_a - 31.9, \quad (2)$$

The associated total errors were calculated taking into account the statistical laws of error propagation.

The Individuation of the Lithotype and Its Possible Sourcing Area

The lithological attribution for each archaeological finding was carried out by combining the Raman spectroscopy results with the mesoscopic observation of the rock structure.

Once the lithology was hypothesised for each sample, the term and their possible sourcing area were researched using the legend of the 1:500.000 "Structural Model of Italy". The wide range of the legend voices was simplified by the definition of a new legend composed of only twelve voices, which comprised all the hypothesised lithology: 1. Amphibolite; 2. Amphibolite with Greenstone; 3. Amphibolite and Granulite; 4. Calcschist; 5. Calcschist with Greenstone; 6. Calcschist with Metabasite; 7. Gabbro; 8. Gabbro and Diorite; 9. Metabasite; 10. Greenstone; 11. Serpentinite; 12. Serpentinite with Greenstone. The term "Greenstone" covers different lithology characterised by the same green colour caused by the presence of green minerals, such as Na-pyroxene rocks, jadeite, omphacite, serpentinite, amphibolite, prasinite, and rocks from the metamorphosed ophiolite complex, such as eclogite, greenschist, amphibolite, granulite, and metabasite [30,31]. Using QGIS technology, the possible primary sourcing areas throughout the Italian peninsula were selected. Therefore, the intersection of polygons with the lines describing the water

courses of the Italian rivers was carried out to highlight the possible secondary supply areas located in northern Italy.

3. Results

3.1. Highlight-Reflectance Transformation Imaging (H-RTI)

The examination of the samples is mainly conducted through the RTI images resulting from the application of the HSH. In addition, among the different enhancing modes provided by the RTIViewer software, a subset is identified as the most useful for the characterisation of superficial discontinuities. The examination of the general appearance of the samples and the detailed description of the specific morphology of peculiar superficial features is carried out using both the Diffuse Gain mode with the maximum Gain and the Normal Visualization mode. Furthermore, the Specular Enhancement mode and Dynamic Multi Light mode are preferred in order to individuate calcium carbonate concretions. The Normal Upsharp Masking mode, with minimum environmental light disturbance (Environment equal to 0) and Gain equal to 4, is applied to facilitate the detection of superficial areas characterised by colour variations from the average tone of the rock.

3.1.1. Sample S1

Surface 1. (Figures 5a and S1) A slightly convex surface is enclosed by superior and lateral regular and rounded edges and a much more irregular but likewise rounded fracture edge. Calcium carbonate concretions are identified near the superior and the left edges and no such presence is evidenced on the right edge. The lower edge has concretions both near the fractured limit and on its inner surface. Small hemispherical depressions approximately 1 cm in diameter are visible randomly distributed on the central part of the rock. With appropriate magnification into the hemispherical concavities, calcium carbonate concretions are also visible. Along the lower edge of the rock, there is a hemispherical depression of about 1 cm in diameter which extends on the fracture surface in the form of two concentric and elongated engravings. Again, concretions are visible on the edge and into the engraved surface. Another hemispherical depression with slightly sloped lateral sides characterises the central sector of the superior edge. Calcium carbonate concretions are noticed on its edge and into the depression.

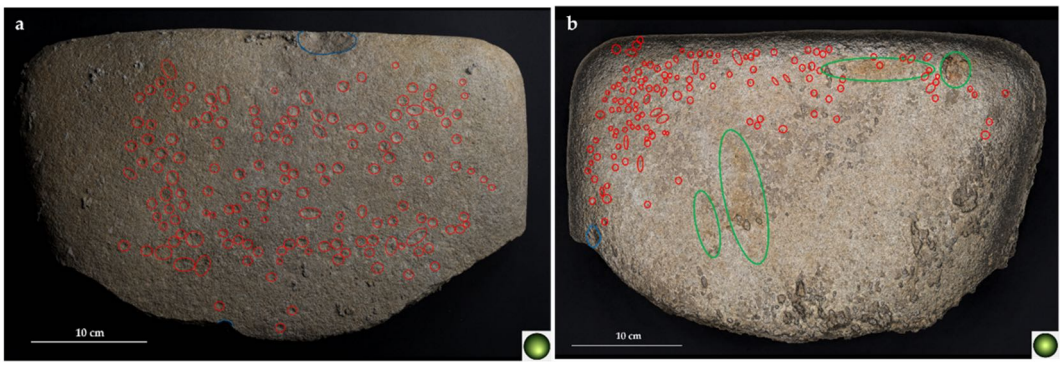

Figure 5. (**a**) Sample S1, surface 1; (**b**) Sample S2, surface 2. The red circle refers to hemispherical concavity, green ellipse to the superficial variation of colour and blue line to depression.

Surface 2. (Figures 5b and S2) The surface does not exhibit surface convexity. The surface shows a considerable number of calcium carbonate concretions in the form of mamillated aggregates mainly concentrated near the lower and right edges. The biggest ones are predominantly detectable in the upper right corner and along the lower edge. Small hemispherical concavities, of about 0.5 cm in diameter, are scattered in the upper left portion of the rock and they sometimes show elongated morphology. Unlike Surface

1, Surface 2 is characterised by four areas where the surface shows a particular brown colour. Interestingly, the colour variation located in the upper right corner also causes the pigmentation of a calcium carbonate concretion aggregate.

3.1.2. Sample S2

A lack of convexity is evident on both rock surfaces. The edges are regular and moderately rounded. Except for the superior rock limit which is covered by lots of aggregates of concretions with a mamillated morphology reaching considerable dimensions, the others do not show these features.

Surface 1. (Figures 6a and S3) Minute hemispherical cavities are visible on the lateral surfaces of the left edge (stressed by white arrows) while the opposite edge is characterised by the same feature along with traces of irregular narrow engravings. Other similar cavities of about 0.5 cm in diameter are signalised in the central part of the rock including three interesting grooves. The superior one (2 × 1 × 0.5 cm) has a semicircular rounded lower edge and gradually decreases in depth to reach the upper part with linear lateral sides. The inferior one is much more defined in shape by linear and precise edges and has a greater depth; its lower limit has a particular bilobed form and it is partially filled by calcium carbonate concretions. Less than 1 cm far from the latter groove, there is another smaller and less deep groove of about 1 cm in diameter. A linear depression is detected as a connection between the two major grooves. It is about 1 cm in width and perpendicularly crossed by a linear dispersion of globular concretions. Near the two inferior grooves, there is an extended area of a light brown colour which is also detected around the superior groove with a less intense colour.

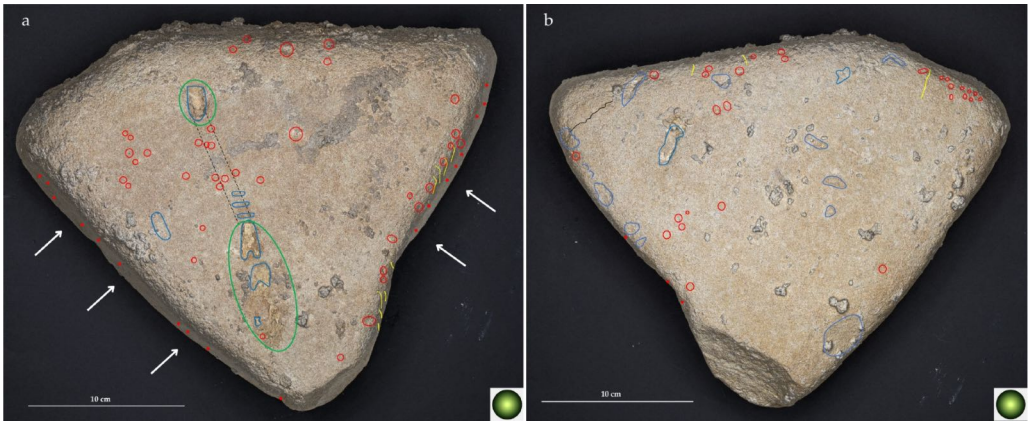

Figure 6. (**a**) Sample S2, surface 1; (**b**) Sample S2, surface 2. The red circle refers to hemispherical concavity, green ellipse to the superficial variation of colour, blue shape to depression, yellow line to linear and sublinear engravings while black line highlights the linear fracture. The black dotted line follows the linear depression connecting the two major grooves.

Surface 2. (Figures 6b and S4) The lower part of the rock is characterised by a discontinuity in its edges, determined by a fracture with rounded edges and small globular calcium carbonate concretions scattered on its edge and upon its inner surface. Rare mamillated aggregates of concretions are also scattered on the overall surface of the rock. Irregular and hemispherical concavities as well as linear short grooves are observed along the upper and the left edges. A superficial linear crack measuring 8 cm in length is observed in the upper left corner of the rock, accompanied by a depression of elongated morphology. At about 5 cm under the crack, there is another similar elongated depression, 2.5 cm in length and 1 cm in width, defined by linear edges and nearly vertical sides. The upper portion

of the depression is filled by concretions which are also detected in the small and rare hemispherical concavities scattered on the rock surface.

3.2. 3D Photogrammetry

Three-dimensional reproductions have a high resolution that guarantees the accurate replication of the superficial fabric of every sample. Nevertheless, it is evident that there is a clear discrepancy in colour between the 3D model elaborated using Agisoft Metashape and the corresponding file uploaded in Sketchfab (Figure 7a). Generally, Sketchfab models are usually darker than the original ones opened using Agisoft Metashape, which are much more like the real colour of the object. The application of colour correction to photographic images is only attempted for BTV photo shooting sessions. The colour accuracy of the 3D model obtained using balanced photos is superior and the appearance of the archaeological finding is faithful to the colour observed by the naked eye. Moreover, the BTV surface examination through the 3D model displays the presence of curvilinear engravings, which are not visible to the naked eye, as highlighted in Figure 7b.

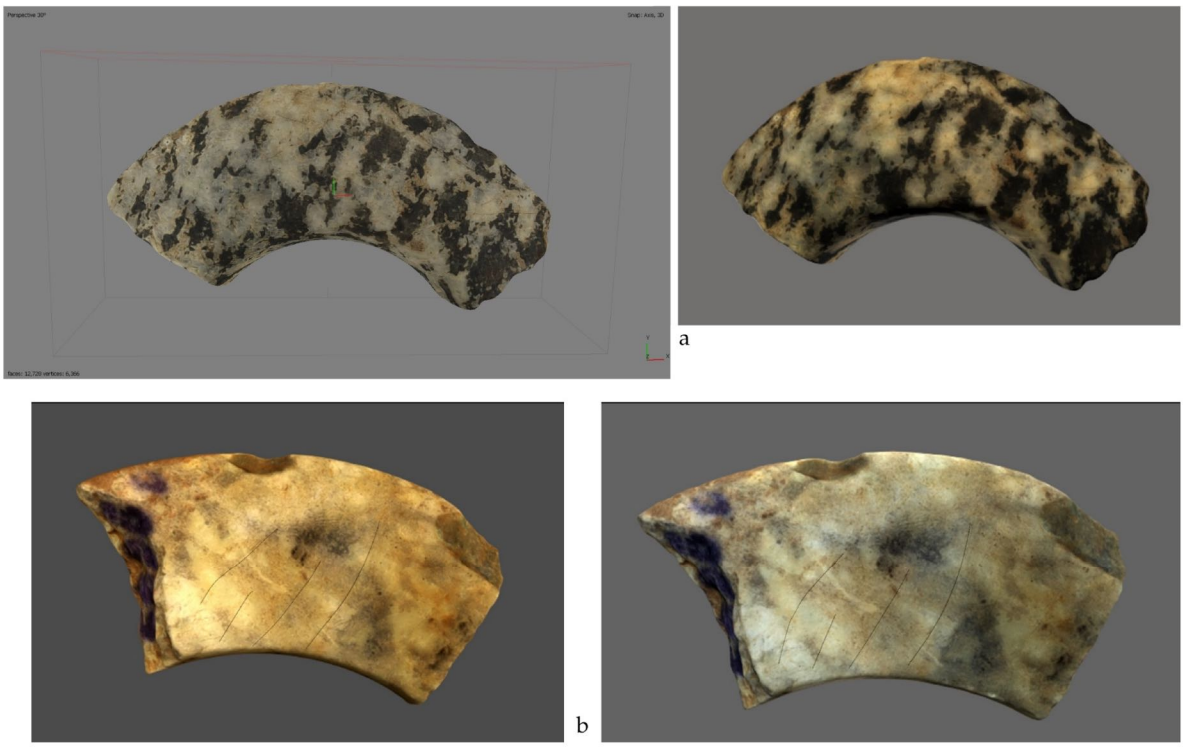

Figure 7. (**a**) The comparison of the R3 sample 3D model in Agisoft Metashape rendering (**left**) and the R3 sample 3D model in Sketchfab (**right**); (**b**) In Sketchfab visualisation, the comparative display of R4 sample 3D model deriving from non-processed photographs (**left**) and R4 sample 3D model from processed photographs (**right**). Dark lines highlight the superficial curvilinear engravings.

All the links to the Sketchfab interactive examination of the archaeological findings are available in Appendix B.

3.3. Raman Spectroscopy

For each sample, spectra of the leucocratic and melanocratic fractions are collected.

Table 4 presents a schematic synthesis of the results for each sample analysed including the hypothesis of the lithological category to which each sample might belong.

Table 4. Summary of Raman results for each sample are reported. Amp: Amphibole; Ats: Anatase; Bt: Biotite; Cal: Calcite; Dps: Diopside; Ep: Epidote; Hem: Hematite; Or: Orthoclase; Prh: Prenhite; Px: Pyroxene; Srp: Serpentine; Tnt: Titanite; Zem: Zemannite; Zeo: Zeolite.

	Leucocratic Fraction		Melanocratic Fraction			
	An (mol%)	Other Minerals	% Px	% Amp	Other Minerals	Lithotype
R1	-	Prh, Cal	70	30	-	Metabasite
R2	23 ± 4	Cal, Or	-	100	Ep	Silicate marble or Calceschist
R3	47 ± 7	Zem	42	48	Ttn, Ep, Zeo, Bt	Diorite/Gabbro with Amphibole or Amphibolite
R5	33 ± 7	-	100	-	Dsp	Diorite or Granulite
R4	-	Srp, Cal, Or	-	100	Hem, Ats	Serpentine schist

From the mesoscopic observation, the samples show high variability in the quantity of the leucocratic and melanocratic fractions. R4 has the highest percentage of the leucocratic fraction which is also evident through its light colour. Regarding the rock structure, R1, R2, and R5 show a moderate foliation. This feature in R2 is observable especially in the two fracture surfaces whereas in R1 and R5 the foliation is highlighted by the preferential spatial orientation of the melanocratic fraction. A preferred orientation of melanocratic minerals is not detectable in R3 and that condition determines the casual fabric of the entire fragment. In contrast with the other samples, the R4 fracture surfaces show a foliation oriented with the profile of its lateral sides.

The Raman spectra analysis shows that the leucocratic fraction of sample R1 mainly consists of prehnite (Prh) and calcite (Cal) while its melanocratic fraction is made of pyroxene and a low percentage of amphibole. The proof of the pyroxene and amphibole discrimination is reported in Figure 8a. Prehnite is an inosilicate of calcium and aluminium resulting from a low-grade metamorphic process, defining the HP-LT metamorphic prehnite-pumpellyite facies. The water content in the prehnite structure determines the characteristic peak at about 3600 cm^{-1} (Figure 8b), which confirms its mineralogical attribution. Calcite in metamorphic rocks is a common mineralogical phase deriving from the transformation of sedimentary protolith containing calcium carbonate. The acquired spectra of calcite highly match the reference spectrum from the RRUFF database (Figure 8b). R1 may be classified as metabasite, deriving from the metamorphism of a basaltic protolith, a basic rock rich in calcium, iron, and magnesium.

Sample R2 predominantly consists of calcite along with a low content of orthoclase and amphibole with epidote. The An(mol%) content is approximately 23 ± 4%, so plagioclases in R2 belong to the Na-rich albitic extreme of the plagioclase solid solution. Epidote and amphibole discrimination is conducted using the fingerprint interval and the different collocation of the hydroxyl groups in the 3200–3800 cm^{-1} region (Figure 8c). The abundance of calcite associated with epidote, a metamorphic mineral, supports the hypothesis that R2 may be a silicate marble or possibly a calcschist.

Considering the leucocratic fraction of samples R3 and R5, it is predominantly made of plagioclase with a respective An(mol%) content of 33 ± 7% and 47 ± 7%. Nevertheless, the percentage of RR5 An(mol%) content does not faithfully represent its bimodal distribution. As the graph in Figure 9 shows, MFP plagioclase composition consists of two domains, the first one at the lower percentage value of 20% and the second one at about 60%, so the Gaussian distribution has a high variance. For this reason, even if the mean value reveals that plagioclases in R5 are albitic (rich in Na), the Ca presence may not be excluded. The average percentage of An(mol%) content in R3 represents the distribution of single values

so the plagioclases of R3 contain both Na and Ca in their mineral structure and fall into the labradorite-andesite interval. Table S1 reports the An(mol%) content of each mineral recognised as plagioclase for R2, R3, and R5. In addition, sample R3 shows the presence of the accessory mineral Zemannite.

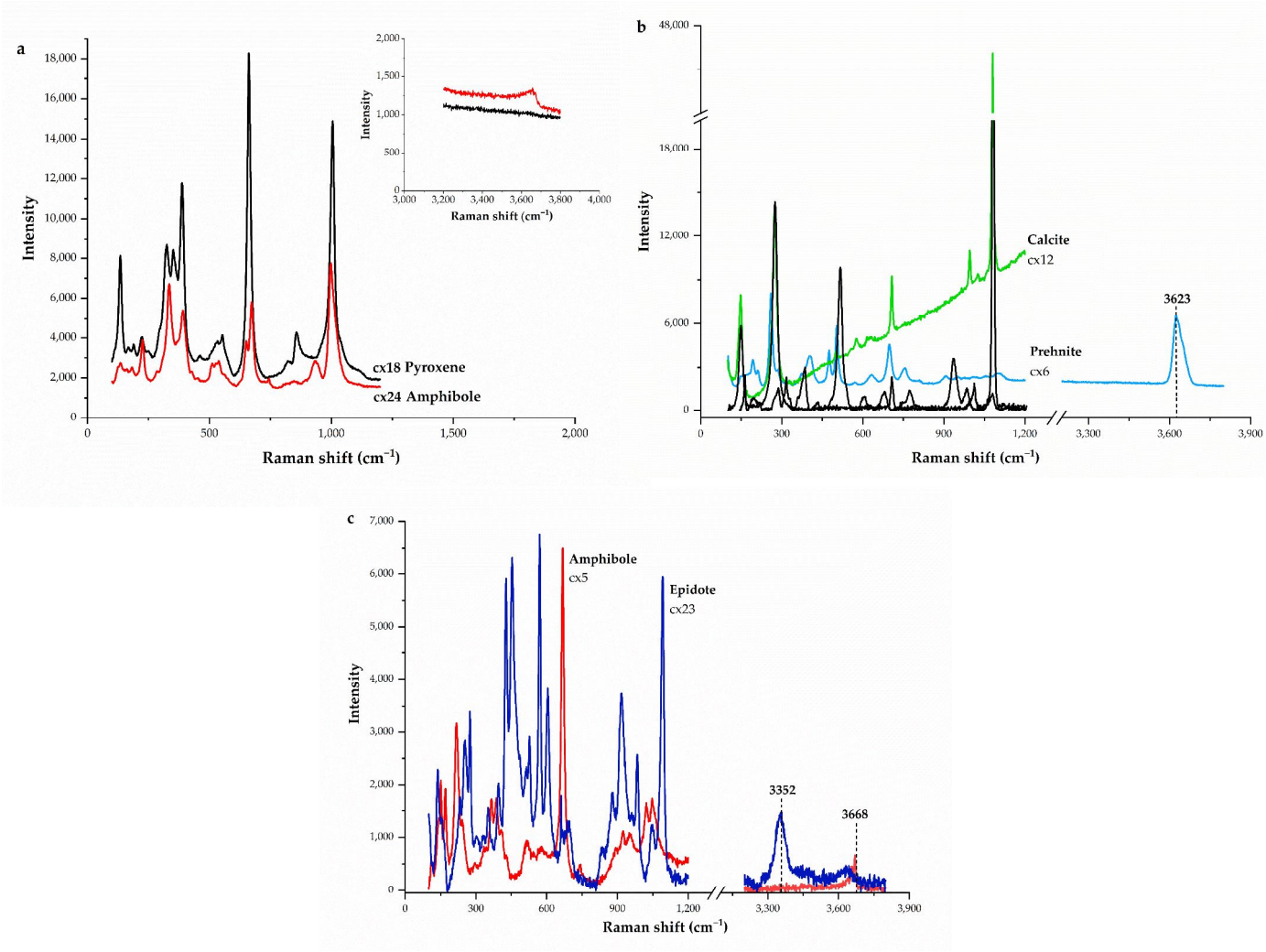

Figure 8. (**a**) Raman spectra of pyroxene (black line) and amphibole (red line) from sample R1. In the upper right corner, the spectral interval associated with the discriminative presence of hydroxyl groups between pyroxene and amphibole. (**b**) Prehnite and calcite spectra from sample R1, which have been identified through the comparison with RRUFF reference spectra (black lines). (**c**) Epidote (blue line) and amphibole (red line) spectra from the sample R2. They mainly differ in the peak position of hydroxyl groups in the 3.200–3.800 cm^{-1}.

Concerning the melanocratic fraction, sample R5 mainly shows the presence of pyroxene, in particular, diopside. The melanocratic fraction of sample R3 is made of pyroxene and amphibole in equal percentages, and minor minerals like epidote, zeolite, brookite, and titanite. The overlapping in the same spectrum of peaks belonging to the amphibole and titanite minerals confirms that titanite in the R3 sample is always an inclusion of amphibole, as shown in Figure 10a.

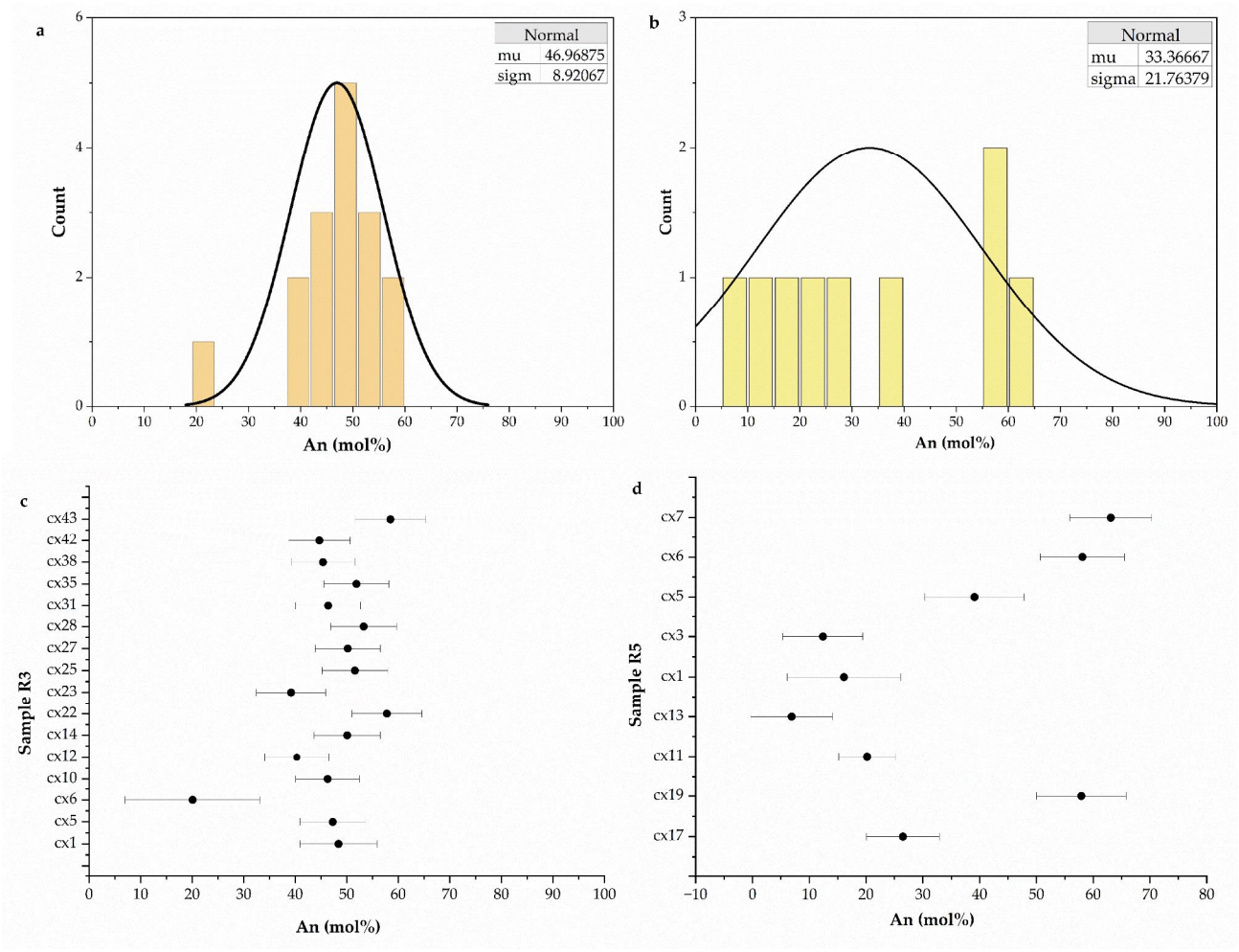

Figure 9. Interval plot with relative errors of the An(mol%) for sample R3 (**a**) and sample R5 (**b**). Gaussian distribution of An(mol%) of the plagioclase fraction for sample R3 (**c**) and R5 sample (**d**).

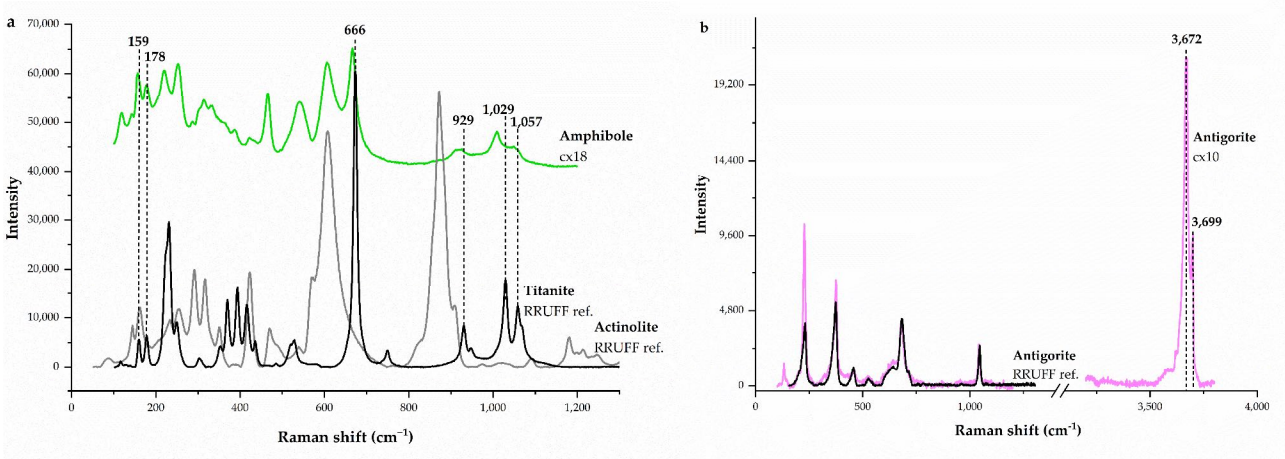

Figure 10. (**a**) Amphibole spectrum acquired from sample R3 (green line). The spectrum is defined by characteristic peaks related to titanite and actinolite reference spectra from the RRUFF database. (**b**) Antigorite spectrum (pink line) from sample R4. There is a clear peak overlapping between the reference spectrum from the RRUFF database (black line) and the characteristic peaks of hydroxyl groups at 3.600–3.700 cm^{-1}.

From the data collected, sample R5 may be classified as a diorite, a magmatic rock with an An(mol%) less than 50%, or a granulite, a metamorphic rock, which may justify the moderately preferred orientation of melanocratic minerals. The uncertainty in the R3 lithological classification derives from its An(mol%) value which is too close to the cutoff value between gabbro and diorite at An(mol%) equal to 50%. For this reason, R3 is simply labelled as a diorite/gabbro rich in amphibole.

Finally, the leucocratic fraction of R4 is composed of a small amount of calcite and orthoclase, a K-feldspar, together with an abundance of antigorite, a mineral belonging to the phyllosilicate serpentinite group usually found in the metamorphosed serpentinites (Figure 10b). The scarce melanocratic fraction consists of amphibole, hematite, and anatase. The abundance of antigorite related to the foliated structure of the rock supports the classification of R4 as a serpentine schist, deriving from the metamorphism of a protolith containing calcium carbonate, which is testified by the presence of calcite in the rock.

Geographical Individuation of Potential Primary and Secondary Sourcing Areas

Throughout the Italian peninsula, five main areas have been selected in the research of the primary and secondary sourcing areas of the lithologies that constitute the samples: the Central Eastern Alps (Retiche Alps and Austrian Alps), the Western Alps, the northern sector of Apennines, the Calabrian Apennines, and the Islands (Nebrodi Mounts, Gennargentu Massif, and the north-eastern portion of Corsica Island). In detail, calcschist frequently associated with greenstone, is highlighted in the Western Alps, from the Maritime to the Pennine Alps, and in the northern Apennines, especially in the Voltri Group and in the External Ligurian Units areas. Metabasite outcrops are situated in the Graie and Cozie Alps sectors, then small outcrops are detected in the south-western portion of the Voltri Group, in the northern sector of the Calabrian Apennine and the Aspromonte massif. Calcschist associated with metabasite is also observed in the Sila Massif plateau and the Gennargentu Massif (Sardinia). In northern Italy, amphibolite and intrusive magmatic rocks, like diorite or gabbro, mainly outcrop in the Pennine Prealps, between Biella and Ivrea, and in the Lepontine Alps. Furthermore, gabbro can be found in the Ligurian Voltri Group area and associated with calcschist outcrops in the External Ligurian Units. Limited outcrops of amphibolite with greenstone are detected in the Maritime Alps, near the Argentera Mount (3.297 m a.s.l.) while amphibolite in much more extended outcrops is situated in Sicily, by the Nebrodi Mounts, and in the Sila Massif plateau as in the Aspromonte Massif. Granulite is found in limited locations within the Pennine and Lepontine Alps while more extended outcrops are in the Sila Massif plateau. Serpentinite is widespread in the Western Alps, in the area enclosed between the Monviso Massif and Mount Cervino, whereas a large outcrop can be found in the Voltri Group between Savona and Genoa. There is serpentinite with greenstone in the Nure Valley and on the right slope of the Trebbia Valley, between the towns of Travo and Bobbio.

The study of secondary sourcing areas is carried out with a precise focus on northern Italy, as shown in Figure 11. The main watercourses and their minor tributaries can be considered secondary sources of rock in the form of cobbles and pebbles. The Po river and especially its minor affluents are highlighted because they directly intersect the geological outcrops and become the fragments' catchment area of the lithologies mentioned above. In detail, the calcschist with greenstone, metabasite, and serpentinite outcrops situated in the Cozie Alps may be transported from the Monviso Massif and the surrounding area by a network of torrents flowing into the Po and Dora Riparia rivers; some tributaries are Rio Bulè, Rio dell'Alpetto, Grana torrent, Variata torrent, Variata of Chianale and Variata of Bellino torrents, and Pellice torrent. From the Graie Alps, calcschist and metabasite may travel from the Orco Valley with its Ribordone tributary, the Malone Valley, the Stura di

Lanzo, and the Dora Riparia River basins, whereas from the upper Graie Alps, serpentinite, amphibolite, and granulite may be carried by the Dora Baltea River basin, thanks to the catchment action of Marmore, Clavalite, Evancon, and Lys torrents. From the Pennine Alps, gabbro and diorite with amphibolite and granulite might be collected by the Sesia and Toce River hydrographic basins. Calcschist and amphibolite cobbles from the Maritime Alps may be respectively carried by the Rio Nero and the Rio Di Valle streams, flowing into the Bormida of Millesimo river and by the Gesso torrent belonging to the Stura di Demonte hydrographic basin. Furthermore, calceschist and serpentinite outcrops in the Ligurian Voltri Group may be collected as pebbles in the Orba Valley and the right slope of Bormida Valley, which crosses Alessandria town. Taro Valley and its Ceno tributary torrent may be characterised by the presence of calcschist and gabbro coming from their outcrops in the External Ligurian Unit. Finally, The Trebbia and Nure valleys may collect serpentinite cobbles from their outcrops in the upper part of the valleys.

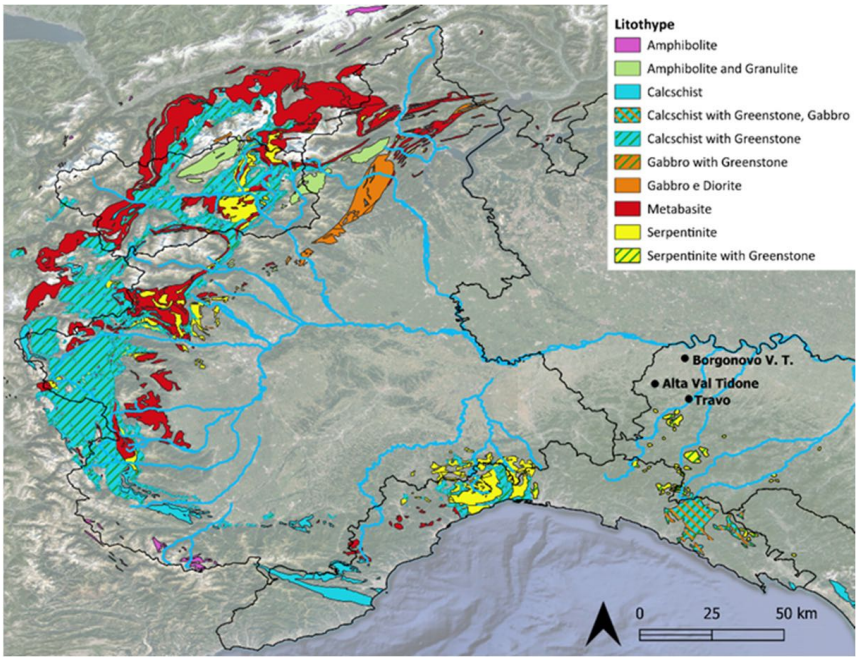

Figure 11. The primary outcrops and the main streams crossing them in northern Italy.

4. Discussion

4.1. Highlight-Reflectance Transformation Imaging (H-RTI)

The Reflectance Transformation Imaging technique has already been recognised as a valuable instrument for the examination of different types of objects in aerial conditions, like paintings [14], coins [17], papyrus [19], or large monuments [62], and further for subaqueous relicts [63]. RTI images are generally used to deepen the knowledge of objects already known for their specific ancient usage [20,21]. The methodology requires the use of basilar photographic instruments and open-source software, which make the technique particularly suitable to users of all levels. The capability of RTI images to facilitate interactive selection of the illumination direction of an object's surface enables researchers to identify traces and details that are not visible to the naked eye. Moreover, the resulting files can be shared and easily visualised by experts using the open-source software RTIViewer. This attitude may prevent archaeological objects from transport and excessive manipulation, which potentially lead to damages [21,64].

In the present study, the resulting images represent the initial element on which the hypothesis regarding the specific archaeological employment may be based. This is

achieved through the elaboration of a comprehensive framework of traces on the object surfaces. In addition, the introduction of a metric reference next to the object into the shooting frame allows reliable measurement of superficial traces in width and height while their depth may not be so accurate due to the Highlight-RTI method of photo acquisition that causes almost 10% error in profilometric measurements [65]. The interpretation method of RTI results elaborated by Toma (2018–2019) [57] allows for the description and the temporal collocation of all the detected superficial traces, particularly through carbonate concretions as an essential proxy. In fact, they form naturally when artefacts are buried, as a result of the calcium carbonate percolation into soils and subsequent precipitation on rough surfaces. Surficial colour variations in both rocks are considered recent natural traces, resulting from the natural deposition on the porous matrix of iron and manganese oxides, which characterise the soils of Travo archaeological site [66]. This consideration is also corroborated by the evidence of fully coloured calcium carbonate concretions on the surface 2 of S1, on which iron oxides precipitate after the formation of concretions during the rock burial. The edges of both rocks have been regularised by distinct natural (for S1) and anthropic (for S2) events, and hemispherical concavities on their surfaces are labelled as ancient tapping marks.

The rectangular shape and the several tapping marks on the plain Surface 2 of S1 lead to the hypothesis that the rock may have been used as a grindstone. In this regard, it may be considered a grindstone due to the medium to fine grain dimensions, which guarantee the right abrasive capacity. However, the tapping marks are not related to striae, which are typical features identifying a rock as a grindstone [67]. Moreover, the convexity of Surface 1 is not a specific feature of a grindstone even though deeper tapping marks are detected. Thus, all the evidence may result from deliberate human manufacture of the entire rock aimed at an as yet undetermined form of employment. The lower fractured edge may be caused by an ancient natural or intentional phenomenon. As regards sample S2, its edge regularisation is testified by the linear engravings along the edges, which may also be considered an effect of human rock manufacturing. The grooves found on the S2 Surface 1 are defined as hits due to their similar shape. They may be generated by the intentional beating of a specific instrument on the surface. The reduced grain dimensions of the rock associated with sparse tapping marks without characteristic striae exclude the possibility that it may be a grindstone. Indeed, its characteristic triangular shape and the evidence of a linear depression connecting the two biggest hits on Surface 2 need an in-depth analysis through comparison with other similar objects.

4.2. 3D Photogrammetry

Photogrammetry is widely employed for its didactic purpose, especially in geological, geomorphological, or mineralogical studies [41] and further for the three-dimensional construction of aerial maps of extended areas, like archaeological sites [42]. Photogrammetry applied to cultural heritage has been limited due to the technical requirements because the process needs the use of professional photographic equipment and specific software for graphic elaboration. The acquisition of such equipment and software often requires significant financial efforts. The application of 3D photogrammetry using the image-based methodology enables the reproduction of all the samples with an acceptable accuracy due to the high quality of the photos captured. Nevertheless, it is recognised that photogrammetry based on laser scanning technology guarantees a higher spatial resolution and accuracy of 3D results than the image-based method [58]. 3D models may be utilised not only for the optical examination of the samples but also for their valorisation. Using Sketchfab—one of the most known and easy-to-use platforms designed for the download and interactive visualisation of 3D models [11]—researchers and archaeologists manage to study and share

artefacts wherever they are working with their computers. Studying artefacts with digital platforms also prevents all the possible exogenous factors that may cause damage due to the manipulation and transport of archaeological findings [64]. Moreover, archaeological heritage valorisation may be carried out by the introduction of digital reproductions into the museum collections through the most common sharing technology, like QRcodes, or digital devices, such as tablets and monitors. On these supports, 3D models can be observed and interactively moved by the users which enhances the quality of the experience offered to visitors by museums [10,12]. In addition, digital reproductions enable the display of artefacts that might be locked in a museum's deposit due to limited exhibition space, the artefact's fragility, and specific requirements for conservation [64]. In this way, 3D models serve also as a useful tool for cultural heritage conservation as they are the digital record of the condition of the object at a specific moment [64].

Three-dimensional models of R1, R2, R3, R4, and R5 obtained in the present study faithfully reproduce the shapes and superficial details of the samples, as demonstrated by the observation of engravings on the BTV surface, which has not been individuated through mesoscopic analysis with the naked eye (see Figure 7b). However, the 3D model colour output usually does not maintain the original sample tone. For this reason, the colour correction of photos through the ColorChecker reference is considered an effective solution, as evidenced by the BTV example (see Figure 7b).

4.3. Raman Spectroscopy

Raman spectroscopy is completely non-invasive and non-destructive, which are fundamental requirements to define it as a suitable chemical technique for cultural heritage analysis [68,69]. It has been widely employed for the examination of different safeguarded objects like pottery, superficial deterioration coating of paintings and metal artefacts, glasses, inks, and human bones [35] whereas a small amount of research has been conducted on lithic archaeological findings [70,71].

The present study interestingly combines qualitative and quantitative analysis of lithic artefacts to carry out the most complete and reliable mineralogical determination of bulk material. In fact, Carey et al. (2015) [40] report an accuracy of 84% for matching entire spectra using CrystalSleuth functionality. In detail, the accuracy of the qualitative matching by CrystalSleuth strongly depends on peak quality and the spectral signal-to-noise ratio [72]. Despite its capacity to enhance the overall peak intensity, the 532 nm laser inevitably affects spectral quality due to its capacity to induce an increase in emitted fluorescence by minerals which is proportional to the fourth power of laser frequency [73]. For all these reasons, the quantitative methodology consolidates the qualitative results by determining the anorthite content (An(mol%)), which is extremely useful for the collocation of minerals into the plagioclase solid solution [61] and then for the discrimination between gabbro and diorite petrographic groups. Moreover, this approach gives the possibility to overcome the subjectivity of the common identification of raw material made through the naked eye observation [74]. In addition, the implementation of Raman spectroscopy results with QGIS technology establishes a methodology to pursue reliable provenance information for lithotypes, avoiding X-ray powder diffraction (XRPD) or SEM analysis, which require specimen treatment to obtain a detailed chemical analysis of trace elements [31,71]. Nevertheless, the surface roughness and shape of MFP impede the accurate acquisition of some spectra and for this reason, its petrographic classification is less accurate than the others. Generally, surface irregularities, superficial patinas, and mineral orientation on the rocks usually change the quality of spectra acquisition and even cause the disappearance or shift of peaks [75].

In detail, the lithologies of R1, R2, R3, and R4 belong to the HP-metaophiolite category, a term that associates different lithologies deriving from the same metamorphic process that occurred on the oceanic crust and the underlying upper mantle during the obduction process [29]. HP-metaophiolite rocks are widely recognised as preferred stones for the lithic industry of northern Italy, especially the so-called "greenstone" for polished stone tools like ring bracelets [22–24,30]. However, during the first VBQ culture, there is evidence of an increase in the regional variability of the type of rock used to realise ornaments and other tools, and the widespread use of "greenstone" was gradually replaced by other lithologies because they are different from the usual greenstone lithotypes [23]. This trend seems to be confirmed by the results of the samples analysed in the present study.

The QGIS examination of the geographical collocation of the lithological outcrops results in a significant overlap with the still-known primary sourcing area of the Monviso Massif and the Voltri Group along with the Beigua Unit [22,23,26–28,31,76]. Regarding the Voltri Group, R1, R3, and R5 may be derived from the Beigua Unit, consisting of metabasites associated with altered peridotites, whereas R2 and R4 may come from the Voltri Unit where serpentinites and calcschists are dominant [77]. The entire arc of the Western Alps may also be a primary supply area for the lithologies mentioned above, as well as for granulite which refers to the R5 sample.

Various valleys are recognised as potential secondary deposits of cobbles and boulders due to the erosive action of the watercourses crossing the geological outcrops. The Rio Bulè Valley, which is widely recognised as the most important quarry area of greenstone [27,28], as well as the Pellice torrent and the Dora Riparia River basins, may be important for serpentinite, calcschist, and metabasite supply. The Sesia hydrographic basin may gather gabbros, diorite, and metabasite. Regarding the Voltri Group, the Orba and Lemme Valley with their tributaries are confirmed as the major supply areas for calcschist, serpentinites, and gabbros [22,31]. Differently from the literature, the Ligurian Units are individuated as a supply area, especially for rocks characterised by metamorphic minerals of the prehnite-pumpellyite facies [78], like the R1 sample. In addition, serpentinites associated with greenstone are interestingly highlighted along the right side of the Trebbia Valley and the Trebbia River may be a potential source of cobbles of serpentinite and lithologies from the ophiolitic complex. The presence of these outcrops close to the archaeological sites suggests that they may have been exploited during the Neolithic age. Nevertheless, especially for ring bracelets, the primary supply area may take precedence over cobble collection from the riverbanks. In fact, the shear stress that occurs during the transport along the watershed causes the intrinsic fragility of cobbles [79], which complicates the subsequent stone manufacturing [23,28].

5. Conclusions

In this study, we have successfully demonstrated the relevance of the analytical techniques employed in solving specific queries formulated for different types of archaeological findings. Techniques have been adapted from their conventional field of study to exploit their potential for archaeological research. Furthermore, the chosen techniques are completely non-invasive and non-destructive, ensuring the integrity of the artefacts, a requisite that is particularly recommended in the cultural heritage context.

In detail, Highlight-Reflectance Transformation Imaging (H-RTI), applied exclusively to samples S1, S2US952_a, and US952_b, enables an in-depth analysis of superficial traces using common photographic equipment and open-source software. In this study, the analytical method for the identification and characterisation of traces has been integrated and standardised, building upon the already defined approach [57]. RTI images allow archaeologists to elaborate upon the most complete framework of superficial traces on

which the definition of the hypothetical ancient usage of the artefacts is set. Moreover, the simple way of sharing RTI models through links and compact files makes the technique effective because it guarantees their continuous detailed study by the archaeologists who collaborated on the research, preventing damage to precious objects.

Photogrammetry and the resulting three-dimensional models have been acknowledged for their dual utility: the accuracy of the 3D reproductions and the possibility of their sharing through the online platform Sketchfab. Like the RTI images, 3D models facilitate the examination of artefacts by different experts across the world, avoiding the necessary transportation of fragile objects. Three-dimensional models also turn into a valorisation instrument for archaeological findings because they might integrate with museum collections by means of QR code technology, links, or interactive monitors.

As regards Raman spectroscopy, despite the surface irregularity of the artefacts and complications occurring during the spectra acquisition, the combination of the qualitative approach with the quantitative method for the estimation of An(mol%) of the plagioclase fraction allows for the lithological determination of all the samples. This method clearly overcomes the high uncertainty of lithological identification through naked-eye observation. Regarding the individuation of the natural sourcing areas for raw material, the Monviso Massif and the Voltri Ligurian Group, which have been long ascertained as supply areas due to the discovery of quarrying activities, have now been integrated with the External Ligurian Unit. This represents a new potential area for the extraction of serpentinites, calcschist, and gabbro associated with greenstone, which are also the lithotypes hypothesised to be the raw materials of samples R2, R3, and R4. This new evidence must be considered by archaeologists, and it appears to be supported by the proximity of the aforementioned geological unit with the archaeological sites where the artefacts have been unearthed.

Supplementary Materials: The following supporting information can be downloaded at: https://www.mdpi.com/article/10.3390/app15031478/s1, Figures S1–S4: additional images of sample S1 and S2 from the RTIViewer visualisation modes; File S1: final report generated by Agisoft Metashape with all the processing parameters adopted during the creation of the sample R2 three-dimensional model; Table S1: An%(mol) content of each mineral belonging to the plagioclase fraction for R2, R3 and R5 samples.

Author Contributions: Conceptualization, L.F., S.P. and L.T.; data curation, L.F.; formal analysis, L.F. and M.Z.; funding acquisition, L.T.; investigation, L.F., S.P., P.F., M.Z. and L.T.; methodology, L.F., S.P., P.F., M.Z. and L.T.; project administration, M.M., P.M. and L.T.; resources, M.M., P.M. and L.T.; supervision, S.P. and L.T.; validation, L.F., S.P., M.M., P.M., P.F., M.Z. and L.T.; writing—original draft preparation, L.F.; writing—review and editing, L.F., S.P., M.M., P.M., P.F., M.Z. and L.T. All authors have read and agreed to the published version of the manuscript.

Funding: This research was internally funded by the University of Milan, Fondo Scavi Archeologici "Maria Teresa Grassi".

Data Availability Statement: The original contributions presented in the study are included in the article/supplementary material, further inquiries can be directed to the corresponding author.

Acknowledgments: The authors are grateful to Francesca Navarro who supported the realisation of the 3D photogrammetric methodology and Professor Roberto Sergio Azzoni for kindly allowing the use of the laboratory for the photographic acquisition. The authors involved in the publication refer to the Superintendence of Archaeology, Fine Arts and Landscape for the Provinces of Parma and Piacenza.

Conflicts of Interest: The authors declare no conflicts of interest.

Appendix A

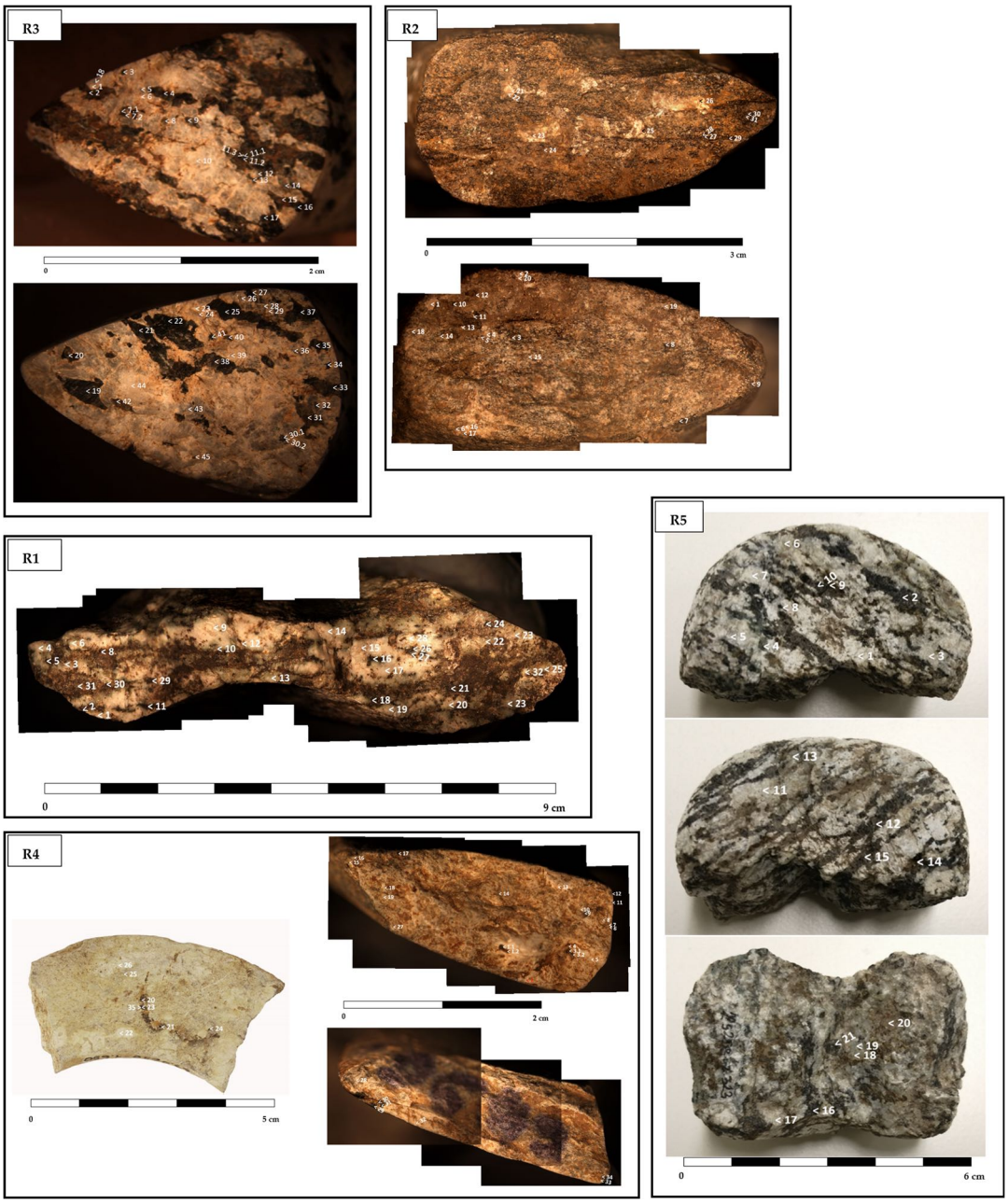

Figure A1. Points of spectral signal collection upon the fractured and polished surfaces of the archaeological artefacts.

Appendix B

Sample R1:
https://skfb.ly/p98IB (accessed on 20 January 2025)
Sample R2:
https://skfb.ly/p98IE (accessed on 20 January 2025)
Sample R3:
https://skfb.ly/p98HW (accessed on 20 January 2025)
Sample R4 (from processed photographs)
https://skfb.ly/p98Is (accessed on 20 January 2025)

Sample R4 (from non-processed photographs)
https://skfb.ly/p98IJ (accessed on 20 January 2025)
Sample R5:
https://skfb.ly/p98IF (accessed on 20 January 2025)

References

1. Larcombe, P.; Ross, P.J.; Fandry, C. Applying Geoarchaeological Principles to Marine Archaeology: A New Reappraisal of the "First Marine" and "in-Situ" Lithic Scatters, Murujuga (Dampier Archipelago), NW Australia. *Geomorphology* **2025**, *468*, 109494. [CrossRef]
2. Pescio, S.; Trombino, L.; Bruni, S. Le Strutture a Ciottoli Combusti Di S. Andrea a Travo: Approccio Geoarcheologico. In *Preistoria e Protostoria dell'Emilia Romagna*; Bernabò Brea, M., Ed.; Istituto Italiano di Preistoria e Protostoria: Florence, Italy, 2016; pp. 249–255.
3. Mcgovern, P.E. Science in Archaeology: A Review. *Am. J. Archaeol.* **1995**, *99*, 79–142. [CrossRef]
4. Otero, J. Heritage Conservation Future: Where We Stand, Challenges Ahead, and a Paradigm Shift. *Global Chall.* **2022**, *6*, 2100084. [CrossRef]
5. Sandu, I. Modern Aspects Regarding the Conservation of Cultural Heritage Artifacts. *Int. J. Conserv. Sci.* **2022**, *13*, 1187–1208.
6. Revedin, A.; Aranguren, B.; Becattini, R.; Longo, L.; Marconi, E.; Lippi, M.M.; Skakun, N.; Sinitsyn, A.; Spiridonova, E.; Svoboda, J. Thirty Thousand-Year-Old Evidence of Plant Food Processing. *Proc. Natl. Acad. Sci. USA* **2010**, *107*, 18815–18819. [CrossRef]
7. Previti, G.; Luci, B.; Lemorini, C. Micro-Photogrammetry and Traceology: New on-Site Documentation Approaches Using Portable Digital Microscopes. *J. Archaeol. Sci.* **2024**, *168*, 106004. [CrossRef]
8. Luo, L.; Wang, X.; Guo, H.; Jia, X.; Fan, A. Earth Observation in Archaeology: A Brief Review. *Int. J. Appl. Eart Obs. Geoinf.* **2023**, *116*, 103169. [CrossRef]
9. Kristiansen, K. Towards a New Paradigm?: The Third Science Revolution and Its Possible Consequences in Archaeology. *Curr. Swed. Archaeol.* **2014**, *22*, 11–34. [CrossRef]
10. Mohd Noor Shah, N.F.; Ghazali, M. A Systematic Review on Digital Technology for Enhancing User Experience in Museums. In *User Science and Engineering*; Abdullah, N., Wan Adnana, W.A., Foth, M., Eds.; Springer: Singapore, 2018; pp. 35–46.
11. Dionisio, G.; Faralli, C.; Jasink, A.M. Funzione e Divulgazione Dei Modelli 3D All'interno Del Museo Interattivo. In *MUSINT 2: Nuove Esperienze di Ricerca e Didattica Nella Museologia Interattiva*; Jasink, A.M., Dionisio, G., Eds.; Firenze University Press: Florence, Italy, 2016; pp. 35–40.
12. Cardaci, A.; Azzola, P.; Sinani Arcienega, J.F.; Versaci, A. La Digitalizzazione Del Patrimonio Culturale: La Collezione Dei 'Lapidei' Del Museo Delle Storie Di Bergamo. In *Transizioni/Transitions*; FrancoAngeli SRL.: Milan, Italy, 2023; pp. 894–912.
13. Liritzis, I.; Al-Otaibi, F.M.; Volonakis, P.; Drivaliari, A. Digital Technologies and Trends in Cultural Heritage. *Mediterr. Archaeol. Archaeom.* **2015**, *15*, 313–332.
14. Manfredi, M.; Bearman, G.; Williamson, G.; Kronkright, D.; Doehne, E.; Jacobs, M.; Marengo, E. A New Quantitative Method for the Non-Invasive Documentation of Morphological Damage in Paintings Using RTI Surface Normals. *Sensors* **2014**, *14*, 12271–12284. [CrossRef]
15. MacDonald, L.; Guerra, M.F.; Pillay, R.; Hess, M.; Quirke, S.; Robson, S.; Hosseininaveh Ahmadabadian, A. Practice-Based Comparison of Imaging Methods for Visualization of Toolmarks on an Egyptian Scarab. In Proceedings of the Lecture Notes in Computer Science (including subseries Lecture Notes in Artificial Intelligence and Lecture Notes in Bioinformatics); Springer: Berlin/Heidelberg, Germany, 2014; Volume 8509 LNCS, pp. 239–246.
16. Mudge, M.; Malzbender, T.; Schroer, C.; Lum, M. New Reflection Transformation Imaging Methods for Rock Art and Multiple-Viewpoint Display. In Proceedings of the The 7th International Symposium on Virtual Reality. Archaeology and Cultural Heritage—VAST, Nicósia, Cyprus, 30 October–4 November 2006; Ioannides, M., Arnold, D., Niccolucci, F., Maria, K., Eds.; 2006.
17. Mudge, M.; Voutaz, J.-P.; Schroer, C.; Lum, M. Reflection Transformation Imaging and Virtual Representations of Coins from the Hospice of the Grand St. Bernard. In Proceedings of the 6th International Symposium on Virtual Reality. Archaeology and Cultural Heritage-VAST, Pisa, Italy, 8–11 November 2005; Mudge, M., Ryan, N., Scopigno, R., Eds.; Eurographics Association: Aire-la-Ville, Switzerland, 2005.
18. Kotoula, E.; Earl, G. Integrated RTI Approaches for the Study of Painted Surfaces. In Proceedings of the 42nd Annual Conference on Computer Applications and Quantitative Methods in Archaeology, Paris, France, 22–25 April 2014; Giligny, F., Djindjian, F., Costa, L., Moscati, P., Robert, S., Eds.; Archeopress: Bicester, UK, 2014; pp. 123–134.
19. Kotoula, E.; Earl, G. Digital Research Strategies for Ancient Papyri: A Case Study on Mounted Fragments of the Derveni Papyrus. In Proceedings of the 42th Annual Conference on Computer Applications and Quantitative Methods in Archaeology, Paris, France, 22–25 April 2014; Giligny, F., Djindjian, F., Costa, L., Moscati, P., Robert, S., Eds.; Archeopress: Bicester, UK, 2014; pp. 145–154.

20. Polkowski, P.L.; Witkowski, P. Reflectance Transformation Imaging. About a Photographic Method for the Documentation and Analysis of Monuments. *Muzealnictwo* **2018**, *59*, 54–62. [CrossRef]
21. Desmond, A.; Cartwright, I.; Allen, R. Documenting Functional Use-Wear on Bone Tools: An RTI Approach. *J. Comput. Appl. Archaeol.* **2021**, *4*, 214–229. [CrossRef]
22. Micheli, R. Raw Materials, Personal Ornaments and Neolithic Groups: Some Observations on Stone Bracelets of Early Neolithic of Northern Italy. In Proceedings of the Congrés Internacional Xarxes al Neolític-Neolithic Networks Rubricatum, Bellaterra, Spain, 2–4 February 2011; Revista del Museu de Gavà: Gavà, Spain, 2012; Volume 5, pp. 241–248.
23. Ribero, M.; Starnini, E. Gli Anelloni Litici Italiani. Nuovi Dati a 40 Anni dalla Prima Sintesi. In Proceedings of the Le quistioni Nostre Paletnologiche più Importanti... Trent'Anni di Tutela e Ricerca Preistorica in Emilia Occidentale; Maffi, M., Bronzoni, L., Mazzieri, P., Eds.; Archeotravo Cooperativa Sociale: Piacenza, Italy, 2019; pp. 121–135.
24. Micheli, R. Similarities and Differences between Italian Early Neolithic Groups: The Role of Personal Ornaments. *Open Archaeol.* **2021**, *7*, 1274–1294. [CrossRef]
25. Tanda, G. Gli Anelloni Litici Italiani. *Preist. Alp. Trento* **1977**, *13*, 111–155.
26. D'amico, C.; Starnini, E. Circulation and Provenance of Neolithic "Greenstone" in Italy. In *JADE. Grandes Haches Alpines du Neolithique Européèn. V et IV Millénaires av. J.-C.*; Pétrequin, P., Cassen, S., Errera, M., Klassen, L., Sheridan, A., Pétrequin, A.-M., Eds.; Les Cahiers de la MSHE Ledoux n.17, Presses Universitaires de France: Comté, France, 2012; Volume Tome 1, pp. 728–748.
27. Pétrequin, P.; Errera, M.; Pétrequin, A.M.; Allard, P. The Neolithic Quarries of Mont Viso, Piedmont, Italy: Initial Radiocarbon Dates. *Eur. J. Archaeol.* **2006**, *9*, 7–30. [CrossRef]
28. Rossi, G.; Errera, M.; Petrequin, P.; Petrequin, A.-M. Un abbozzo di anellone in pietra verde da Bobbio (PC). *Boll. Stor. Piacentino* **2008**, *100*, 185–202.
29. Rolfo, F.; Benna, P.; Cadoppi, P.; Castelli, D.; Favero-Longo, S.E.; Giardino, M.; Balestro, G.; Belluso, E.; Borghi, A.; Cámara, F.; et al. The Monviso Massif and the Cottian Alps as Symbols of the Alpine Chain and Geological Heritage in Piemonte, Italy. *Geoheritage* **2015**, *7*, 65–84. [CrossRef]
30. D'amico, C.; Starnini, E.; Gasparotto, G.; Ghedini, M. Eclogites, Jades and Other HP-Metaophiolites Employed for Prehistoric Polished Stone Implements in Italy and Europe. *Period. Miner.* **2003**, *73*, 17–42.
31. Giustetto, R.; Venturino, M.; Barale, L.; d'Atri, A.; Compagnoni, R. The Neolithic Greenstone Industry of Brignano Frascata (Italy): Archaeological and Archaeometric Study, Implications and Comparison with Coeval Sites in the Grue, Ossona and Curone Valleys. *J. Archaeol. Sci. Rep.* **2017**, *14*, 662–691. [CrossRef]
32. Starnini, E.; Biagi, P.; Mazzucco, N. The Beginning of the Neolithic in the Po Plain (Northern Italy): Problems and Perspectives. *Quat. Int.* **2018**, *470*, 301–317. [CrossRef]
33. Malone, C. The Italian Neolithic: A Synthesis of Research. *J. World Prehist.* **2003**, *17*, 235–312. [CrossRef]
34. Tinè, V.; Vidale, A. Rivoluzione Neolitica. La conquista di un mondo nuovo. *Archeo. Attualità del Passato.* **2014**, *347*, 78–99.
35. Caggiani, M.C.; Colomban, P. Raman Microspectroscopy for Cultural Heritage Studies. *Phys. Sci. Rev.* **2019**, *3*, 20180007.
36. Vandenabeele, P.; Donais, M.K. Mobile Spectroscopic Instrumentation in Archaeometry Research. *Appl. Spectrosc.* **2016**, *70*, 27–41. [CrossRef] [PubMed]
37. Casadio, F.; Daher, C.; Bellot-Gurlet, L. Raman Spectroscopy of Cultural Heritage Materials: Overview of Applications and New Frontiers in Instrumentation, Sampling Modalities, and Data Processing. *Top. Curr. Chem.* **2016**, *374*, 161–211. [CrossRef] [PubMed]
38. Buzgar, N.; Apopei, A.I.; Diaconu, V.; Buzatu, A. The Composition and Source of the Raw Material of Two Stone Axes of Late Bronze Age from Neamț County (Romania)-A Raman Study. *Analele Stiintifice Univ. "Al. I. Cuza" Iasi Ser. Geol.* **2013**, *59*, 5–22.
39. Hernández, I.; Jorge-Villar, S.; Ferrón, C.C.; Medianero, F.J.; Ramos, J.; Weniger, G.-C.; Domínguez-Bella, S.; Linstaedter, J.; Cantalejo, P.; Espejo, M.; et al. Raman Spectroscopy Analysis of Palaeolithic Industry from Guadalteba Terrace River, Campillos (Guadalteba County, Southern of Iberian Peninsula). *J. Raman Spectrosc.* **2012**, *43*, 1651–1657. [CrossRef]
40. Carey, C.; Boucher, T.; Mahadevan, S.; Bartholomew, P.; Dyar, M.D. Machine Learning Tools Formineral Recognition and Classification from Raman Spectroscopy. *J. Raman Spectrosc.* **2015**, *46*, 894–903. [CrossRef]
41. Aristov, M.M.; Moore, J.W.; Berry, J.F. Library of 3D Visual Teaching Tools for the Chemistry Classroom Accessible via Sketchfab and Viewable in Augmented Reality. *J. Chem. Educ.* **2021**, *98*, 3032–3037. [CrossRef]
42. Marín-Buzón, C.; Pérez-Romero, A.; López-Castro, J.L.; Jerbania, I.B.; Manzano-Agugliaro, F. Photogrammetry as a New Scientific Tool in Archaeology: Worldwide Research Trends. *Sustainability* **2021**, *13*, 5319. [CrossRef]
43. Bretzke, K.; Conard, N.J. Evaluating Morphological Variability in Lithic Assemblages Using 3D Models of Stone Artifacts. *J. Archaeol. Sci.* **2012**, *39*, 3741–3749. [CrossRef]
44. Piana Agostinetti, N.; Faccenna, C. Deep Structure of Northern Apennines Subduction Orogen (Italy) as Revealed by a Joint Interpretation of Passive and Active Seismic Data. *Geophys. Res. Lett.* **2018**, *45*, 4017–4024. [CrossRef]
45. Vai, G.B.; Martini, I.P. Geomorphologic Setting. In *Anatomy of an Orogen: The Apennines and Adjacent Mediterranean Basins*; Springer: Dordrecht, The Netherlands, 2001; pp. 1–4.

46. Conti, P.; Cornamusini, G.; Carmignani, L.; Pizziolo, M.; Daniele, G.; Lavorini, G.; Motti, A.; Natali, N.; Bettucci, C.; Pirro, A.; et al. *Carta Geologica Delle Regioni Emilia-Romagna. Marche. Toscana e Umbria. Scala 1:250.000. Note Illustrative*; Archivio cartografico della regione Emilia-Romagna: Bologna, Italy, 2019.
47. Ferrando, A.; Faccini, F.; Coratza, P. Ophiolites: Geological Heritage with Multifaceted Cultural Values. *Geoheritage* **2024**, *16*, 108. [CrossRef]
48. Amorosi, A.; Fontana, A.; Antonioli, F.; Primon, S.; Bondesan, A. Post-LGM Sedimentation and Holocene Shoreline Evolution in the NW Adriatic Coastal Area. *GeoActa* **2008**, *7*, 41–67.
49. Conti, P.; Cornamusini, G.; Carmignani, L. An Outline of the Geology of the Northern Apennines (Italy), with Geological Map at 1:250,000 Scale. *Ital. J. Geosci.* **2020**, *139*, 149–194. [CrossRef]
50. Maffi, M. Il Neolitico Recente Emiliano (NRE): Proposta di definizione. *Riv. Sci. Preist. LXIV* **2014**, *2014*, 25–55.
51. Bernabò Brea, M.; Miari, M.; Steffè, G. Il Neolitico Dell'Emilia Romagna. In *Preistoria e Protostoria dell'Emilia-Romagna-I. Bernabò Brea, M., Ed.*; Istituto Italiano di Preistoria e Protostoria: Florence, Italy, 2017; Volume 3, pp. 119–137.
52. Gunawardane, P.; Wang, O.; Scher, S.; Rickards, I.; Davis, J.; Malzbender, T. Optimized Image Sampling for View and Light Interpolation. In Proceedings of the 10th International Symposium on Virtual Reality, Archeology and Cultural Heritage VAST, St. Julians, Malta, 22–25 September 2009; Debattista, K., Perlingieri, C., Pitzalis, D., Spina, S., Eds.; 2009.
53. Fiorini, A. Il Metodo Fotografico RTI (Reflectance Transformation Imaging) per la Documentazione delle Superfici Archeologiche. L'applicazione ai Materiali di Età Protostorica. *Archeol. Calc.* **2018**, *29*, 241–258.
54. Cultural Heritage Imaging. *Reflectance Transformation Imaging: Guide to Highlight Image Capture.* Available online: http://culturalheritageimaging.org/downloads/ (accessed on 15 December 2024).
55. Ponchio, F.; Corsini, M.; Scopigno, R. RELIGHT: A Compact and Accurate RTI Representation for the Web. *Graph. Models* **2019**, *105*, 101040. [CrossRef]
56. Cultural Heritage Imaging. Reflectance Transformation Imaging: Guide to Highlight Image Processing. Available online: https://culturalheritageimaging.org/What_We_Offer/Downloads/rtibuilder/RTI_hlt_Processing_Guide_v14_beta.pdf (accessed on 15 December 2024).
57. Toma, A.L. Metodologia RTI per l'identificazione e La Caratterizzazione Delle Tracce Di Utilizzo Sulla Superficie Di Reperti Archeologici. Bachelor's Thesis, Science and Technology for the Environment and Nature, University of Milan, Milan, Italy, 2019.
58. Lastilla, L.; Ravanelli, R.; Ferrara, S. 3D High-Quality Modeling of Small and Complex Archaeological Inscribed Objects: Relevant Issues and Proposed Methodology. *Int. Arch. Photogramm. Remote Sens. Spat. Inf. Sci.* **2019**, *42.2/W11*, 699–706. [CrossRef]
59. Apopei, A.I.; Buzgar, N.; Buzatu, A.; Maftei, A.E.; Apostoae, L. Digital 3D Models of Minerals and Rocks in a Nutshell: Enhancing Scientific, Learning, and Cultural Heritage Environments in Geosciences by Using Cross-Polarized Light Photogrammetry. *Carpathian J. Earth Environ. Sci.* **2021**, *16*, 237–249. [CrossRef]
60. Apopei, A.I.; Buzgar, N. The Raman Study of Amphiboles. *Anal. Stiintifice Univ. AI Cuza Iasi. Sect. 2 Geol.* **2010**, *56*, 57.
61. Bersani, D.; Aliatis, I.; Tribaudino, M.; Mantovani, L.; Benisek, A.; Carpenter, M.A.; Gatta, G.D.; Lottici, P.P. Plagioclase Composition by Raman Spectroscopy. *J. Raman Spectrosc.* **2018**, *49*, 684–698. [CrossRef]
62. Dellepiane, M.; Corsini, M.; Callieri, M.; Scopigno, R. High Quality PTM Acquisition: Reflection Transformation Imaging for Large Objects. In Proceedings of the 7th International Symposium on Virtual Reality, Archeology and Intelligent Cultural Heritage, Nicosia, Cyprus, 30 October–4 November 2006; Ioannides, M., Arnold, D., Niccolucci, F., Mania, K., Eds.; VAST. Eurographics Association: Goslar, Germany, 2006.
63. Selmo, D.; Sturt, F.; Miles, J.; Basford, P.; Malzbender, T.; Martinez, K.; Thompson, C.; Earl, G.; Bevan, G. Underwater Reflectance Transformation Imaging: A Technology for in Situ Underwater Cultural Heritage Object-Level Recording. *J. Electron. Imaging* **2017**, *26*, 011029. [CrossRef]
64. Hanke, K.; Moser, M.; Grimm-Pitzinger, A.; Goldenberg, G.; Toechterle, U. Enhanced Potential for the Analysis of Archaeological Finds Based on 3D Modeling. *Int. Arch. Photogrammetry. Remote Sens. Spat. Inf. Sci.* **2008**, *37*, 187e192.
65. Verni, E.; Fiocco, G.; Grifoni, E.; Lippolis, G.; Ludwig, N.; Malagodi, M.; Pisani, M.; Rovetta, T.; Zucco, M.; Gargano, M. Quantitative Evaluation of the Reflectance Transformation Imaging and Normal Integration Technique in Profilometric Application. *J. Phys. Conf. Ser.* **2022**, *2204*, 012069. [CrossRef]
66. Pescio, S.; Maffi, M.; Trombino, L. Studi Micromorfologici nel Sito Neolitico di S. Andrea a Travo (PC): Ricostruzione della Stratigrafia. In Proceedings of the "...le Quistioni Nostre Paletnologiche più Importanti...Trent'Anni di Tutela e Ricerca Archeologica in Emilia Occidentale. Atti del Convegno (Parma 8-9 giugno 2017); Maffi, M., Bronzoni, L., Mazzieri, P., Eds.; Archeotravo: Piacenza, Italy, 2019; pp. 81–101.
67. Revedin, A.; Aranguren, B.; Gennai, M.; Mariotti Lippi, M.; Pallecchi, P. The Processing of Plant Food in the Palaeolithic. New Data from the Analysis of Experimental Grindstones and Flour. *Riv. Sci. Preist.* **2017**, *67*, 5–18.
68. Kadlecíková, M.; Breza, J.; Vanco, L.; Gregor, M.; Bazovskỳ, I. Raman Spectroscopy of Ancient Beads from Devín Castle near Bratislava and of Four Intaglios from Other Archaeological Finds in Slovakia. *J. Gemmol.* **2015**, *34*, 510–517. [CrossRef]

69. Rousaki, A.; Moens, L.; Vandenabeele, P. Archaeological Investigations (Archaeometry). *Phys. Sci. Rev.* **2018**, *3*, 20170048. [CrossRef]
70. Fornasini, L.; Mantovani, L.; Bertolini, M.; Conversi, R.; Bersani, D. Multi-analytical Characterization of Archaeological Fragments of Pietra Ollare from the Medieval Site 'Piana Di S. Martino' (Piacenza, Italy): A Mobile and Laboratory Approach. *J. Raman Spectrosc.* **2024**, *55*, 232–245. [CrossRef]
71. Gallello, G.; Setien, J.; Cisneros, M.; Valls-Mompó, M.; Martín-Ramos, P.; Palomar, M.E.O.; Peralta, J.Á.P.; Pastor, A.; Marín-Arroyo, A.B. "Natural or Synthetic": The Identification History of an Object in an Archaeological Context. *Microchem. J.* **2024**, *207*, 112088. [CrossRef]
72. Bartholomew, P.R.; Dyar, M.D.; Brady, J.B. The Role of Intensity and Instrument Sensitivity in Raman Mineral Identification. *J. Raman Spectrosc.* **2015**, *46*, 889–893. [CrossRef]
73. Skoog, D.A.; Holler, F.J.; Crouch, S.R. *Principles of Instrumental Analysis*, 6th ed.; Cengage Learning: Boston, MA, USA, 2007.
74. Martínez-Sevilla, F.; Baysal, E.L.; Micheli, R.; Ifantidis, F.; Lugliè, C. A Very Early "Fashion": Neolithic Stone Bracelets from a Mediterranean Perspective. *Open Archaeol.* **2021**, *7*, 815–831. [CrossRef]
75. Waeselmann, N.; Schlüter, J.; Malcherek, T.; Della Ventura, G.; Oberti, R.; Mihailova, B. Nondestructive Determination of the Amphibole Crystal-Chemical Formulae by Raman Spectroscopy: One Step Closer. *J. Raman Spectrosc.* **2020**, *51*, 1530–1548. [CrossRef]
76. Bernabò Brea, M.; Errera, M.; Mazzieri, P.; Occhi, S.; Petrequin, P. Alpine Axeheads in the Square-Mouthed Pottery Culture of Western Emilia: Contexts, Typology and Raw Material Origin. In *Les Haches en Jades. De l'Italie à l'Atlantique*; Petrequin, P., Cassen, S., Errera, M., Klassen, L., Sheridan, A., Petrequin, A.-M., Eds.; Les cahiers de la MSHE Ledoux n.17, Presses Universitaires de France: Comté, France, 2012; pp. 822–871.
77. Boulart, C.; Chavagnac, V.; Monnin, C.; Delacour, A.; Ceuleneer, G.; Hoareau, G. Differences in Gas Venting from Ultramafic-Hosted Warm Springs: The Example of Oman and Voltri Ophiolites. In *Les Haches en Jades. De l'Italie à l'Atlantique*; Petrequin, P., Cassen, S., Errera, M., Klassen, L., Sheridan, A., Petrequin, A.-M., Eds.; Les cahiers de la MSHE Ledoux n.17, Presses Universitaires de France: Comté, France, 2012; pp. 822–871.
78. Marroni, M.; Molli, G.; Montanini, A.; Ottria, G.; Pandolfi, L.; Tribuzio, R. The External Ligurian Units (Northern Apennine, Italy): From Rifting to Convergence of a Fossil Ocean-Continent Transition Zone. *Ofioliti* **2002**, *27*, 119–131.
79. Petit, F.; Houbrechts, G.; Peeters, A.; Hallot, E.; Van Campenhout, J.; Denis, A.C. Dimensionless Critical Shear Stress in Gravel-Bed Rivers. *Geomorphology* **2015**, *250*, 308–320. [CrossRef]